

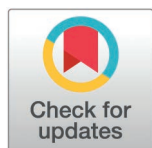
RESEARCH ARTICLE

# Innovation of eco-friendly TiO<sub>2</sub> nano catalyst for new pyrimidine carbonitriles candidates, assessed for significant antioxidant activity, anti-inflammatory effects, and by insilico studies

Wesam S. Shehab<sup>1\*</sup>, Ahmed F. EL-Farargy<sup>1</sup>, Abdel Rahman B. A. El-Gazzar<sup>2</sup>, Hend A. Haikal<sup>1</sup>, Samar M. Mouneir<sup>3</sup>, Abdul-Hamid M. Emwas<sup>4</sup>, Mariusz Jaremko<sup>5</sup>, Magda H. Abdellattif<sup>6\*</sup>

**1** Department of Chemistry, Faculty of Science, Zagazig University, Zagazig, Egypt, **2** Department of Organic Chemistry, National Research Centre, Dokki, Cairo, Egypt, **3** Department of Pharmacology, Faculty of Veterinary Medicine, Cairo University, Cairo, Egypt, **4** Core Labs, King Abdullah University of Science and Technology (KAUST), Thuwal, Saudi Arabia, **5** Biological and Environmental Science and Engineering (BESE), King Abdullah University of Science and Technology (KAUST), Thuwal, Saudi Arabia, **6** Department of Chemistry, Sciences College, University College of Taraba, Taif University, Taif, Saudi Arabia

\* [wsshehab@zu.edu.eg](mailto:wsshehab@zu.edu.eg) (WSH); [m.hasan@tu.edu.sa](mailto:m.hasan@tu.edu.sa) (MHA)



## OPEN ACCESS

**Citation:** Shehab WS, EL-Farargy AF, El-Gazzar ARBA, Haikal HA, Mouneir SM, Emwas A-HM, et al. (2025) Innovation of eco-friendly TiO<sub>2</sub> nano catalyst for new pyrimidine carbonitriles candidates, assessed for significant antioxidant activity, anti-inflammatory effects, and by insilico studies. PLoS One 20(5): e0313959. <https://doi.org/10.1371/journal.pone.0313959>

**Editor:** Ahmed A. Al-Karmalawy, University of Mashreq, IRAQ

**Received:** June 9, 2024

**Accepted:** November 3, 2024

**Published:** May 29, 2025

**Copyright:** © 2025 Shehab et al. This is an open access article distributed under the terms of the [Creative Commons Attribution License](https://creativecommons.org/licenses/by/4.0/), which permits unrestricted use, distribution, and reproduction in any medium, provided the original author and source are credited.

**Data availability statement:** All relevant data are within the paper and its [Supporting Information](#) files.

**Funding:** The research was funded by Taif University Saudi Arabia, project number TU-DSPP-2024-19.

## Abstract

Production of titanium dioxide nanoparticles (TiO<sub>2</sub>- NPs) is carried out in high quantities for an extensive range of applications. These nanoparticles have various physicochemical properties, which can affect their bioactivity. The Biginelli synthesis of 4-cyanobenzaldehyde, ethyl cyanoacetate, and thiourea in the presence of TiO<sub>2</sub> nanoparticle yields 4-(4-cyanophenyl)-6-oxo-2-thioxohexahydropyrimidine-5-carbonitrile (**1**). This multi-component system is safe, eco-friendly, and non-toxic. The introduction of the new system saves time and reduces chemical usage. Compound (**1**) underwent reactions with various additional compounds such as (methyl iodide, chloroacetonitrile, chloroacetone, acrylonitrile, ethyl chloroacetate, and chloroacetic acid/benzaldehyde). The newly synthesized compounds possess remarkable anti-inflammatory and antioxidant activities, making them an excellent choice for therapeutic use.. The in-silico studies include molecular docking using MOE, Pharmacokinetics using Toxoradar, SAR, and DFT studies.

## Introduction

The rise of nanotechnology and eco-friendly chemical synthesis has revolutionized the use of nanoparticles in a multitude of industries. From producing antibacterial materials to enhancing drug delivery systems and creating sunblock to perfecting makeup and microchip technology, nanoparticles have become vital in achieving optimal results. As pyrimidine is a ring involved in DNA and RNA, this indicates higher pharmacological activities; some of the most significant are anticancer, antiviral, particularly anti-HIV, antimicrobial, anti-inflammatory, and antioxidant activities [1–11]. Creating new candidates of pyrimidine thione derivatives with potential

**Competing interests:** The authors have declared that no competing interests exist.

pharmacological effects is one of our aims. Regarding heterogeneous catalysis, the catalyst recovery and separation from the reaction matrix were considered by utilizing various supporting catalysts to restrain the particle and provide a suitable surface area. [12]. The Biginelli synthesis, which produces pyrimidine compounds, has been extensively studied in recent decades, particularly because of the therapeutic properties of the resulting compounds, which include calcium channel blockers, anticancer, antiviral, antimicrobial, anti-inflammatory, and antioxidant compounds [13–14]. **This approach creates a stable and solid framework for the heterogeneous catalyst, which is not soluble in the solution matrix.** [15].

Due to cost-effective synthesis modes, various heterogeneous catalysts such as TiO<sub>2</sub>, Al<sub>2</sub>O<sub>3</sub>, ZrO<sub>2</sub>, and ZnO are being manufactured and have become widely available. For example, TiO<sub>2</sub> is a heterogeneous catalyst used in fuel processing due to its tunable porous surface, high thermal stability, and mechanical strength. [16]. On the other hand, the pharmaceutical industry has resorted to several strategies to improve these compounds for use as drugs. DPPH is a free radical that may be used to determine radical scavenging and related antioxidant activities [17]. The antioxidants help prevent and reduce damage from free-radical reactions because of their ability to donate electrons that can neutralize the formation of free radicals [4,18,19]. Inflammation is a reaction to injury of living tissues, comprising systemic and local responses [20]. Inflammation is also a cellular reaction to harmful stimuli and infections. This physiological response includes delivering blood components to the local site of infection or injury, triggering vasodilation and increased vascular permeability. While inflammation is a healing response of the living body, the body cannot continuously regulate this response, and inflammatory excess can threaten the body. Thus, by understanding how inflammation functions, we may better understand its significance in maintaining our health while helping us discover new anti-inflammatory therapeutics. The hemolytic method is well-known in the biological assessment of anti-inflammatory compounds [21,22], and using the hemolytic and other techniques, the present paper reports the synthesization and characterization of pyrimidine carbonitrile derivatives, which are known as good, dual nature antioxidant and anti-inflammatory drugs. Molecular docking within a molecular operating environment MOE (2019), DFT with Spartan 20, and SAR (structure-activity relationship and pharmacokinetics) are also applied using Molinspiration and Toxiradar [23–25].

## 2. Results and discussion

### 2.1. Nanoparticles titanium dioxide

[Fig 1](#) represents the XRD pattern of the produced nano-TiO<sub>2</sub>, revealing diffraction peaks at  $2\theta = 25$  and  $48^\circ$ ; TiO<sub>2</sub> was recorded in the anatase phase. [26]. The peaks are in an upright position in

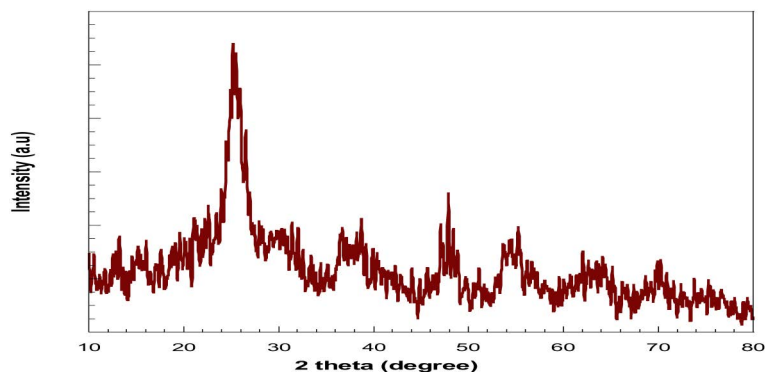


**Fig 1.** XRD pattern of TiO<sub>2</sub>.

<https://doi.org/10.1371/journal.pone.0313959.g001>

agreement with the standard spectrum (JCPDS № 01-089-4921); one can notice that the intensity of the diffraction pattern of the TiO<sub>2</sub> is directly proportional to the reduction of the particle size. This result indicates the formation of the nano-TiO<sub>2</sub> [27]. At the same time, the expected diffraction signal of the rutile phase at 27.5 ° was not detected, which indicated that the formed TiO<sub>2</sub> was only of a particular anatase phase. [28].

Ultrastructural imaging via transmission electron microscopy (TEM) was used to examine the nanocrystals' crystalline phases, size, and aggregation. The TEM images of the catalysts confirmed that the TiO<sub>2</sub> comprises combinations of mostly spherical nanoparticles with an average diameter of ~5 nm. Therefore, TEM was used to supplement the examination of the particle size, crystallinity, and morphology of the TiO<sub>2</sub> [29]; Fig 2 shows TEM images of TiO<sub>2</sub> in anatase phases. The area electron diffraction (SAED) patterns of the nano TiO<sub>2</sub> powder display typical rings that match the anatase phase. The brightness and intensity of the call signals are weak, meaning that TiO<sub>2</sub> was poorly crystallized and partially amorphous.

## 2.2 Chemistry

Synthesis of new heterocyclic molecules was carried out depending on the pyrimidine moiety. The starting material 4-(4-cyanophenyl)-6-oxo-2-thioxohexahydropyrimidine-5-carbonitrile (**1**) was produced using two methods. The optimized reaction conditions are represented in Table 1. The traditional method involves the reaction of thiourea and ethyl cyanoacetate with 4-cyanobenzaldehyde in the presence of a few drops of triethylamine in ethanol under reflux conditions. The reaction of the three components of the TiO<sub>2</sub> nanoparticles (TiO<sub>2</sub>-NPs) as a catalytic amount in ethanol under reflux was archived to obtain Compound (**1**) with optimal reaction conditions (Scheme 1). Infrared (IR), proton, and carbon-13 nuclear magnetic resonance (<sup>1</sup>H-NMR and <sup>13</sup>C-NMR) were used to elucidate Structure (**1**). The IR spectra showed the presence

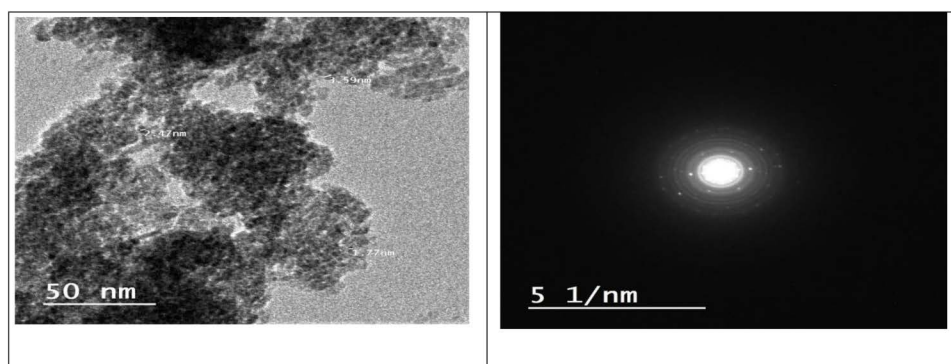


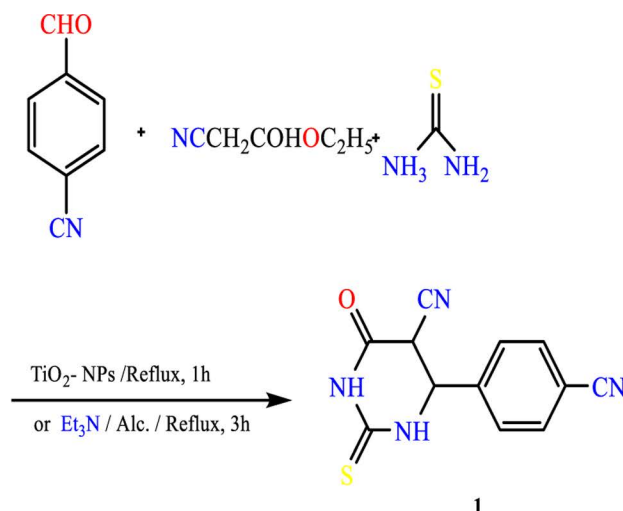
Fig 2. TEM micrograph and SAED of TiO<sub>2</sub>.

<https://doi.org/10.1371/journal.pone.0313959.g002>

Table 1. Optimized reaction conditions.

Compound	Solvent	Catalyst (base)	Temperature (°C)	Time (h)	Yield (%)
1	Ethanol	TEA	Reflux	3	35
1	Ethanol	TiO <sub>2</sub>	Reflux	1	40
2	Ethanol	NaOEt	Reflux	3	60
2	Ethanol	TiO <sub>2</sub>	Reflux	2	72
5	Ethanol	Pyridine	Reflux	5	45
5	Ethanol	TiO <sub>2</sub>	Reflux	3	57

<https://doi.org/10.1371/journal.pone.0313959.t001>



**Scheme 1: Synthesis of 4-(4-cyanophenyl)-6-oxo-2-thioxohexahydropyrimidine-5-carbonitrile.**

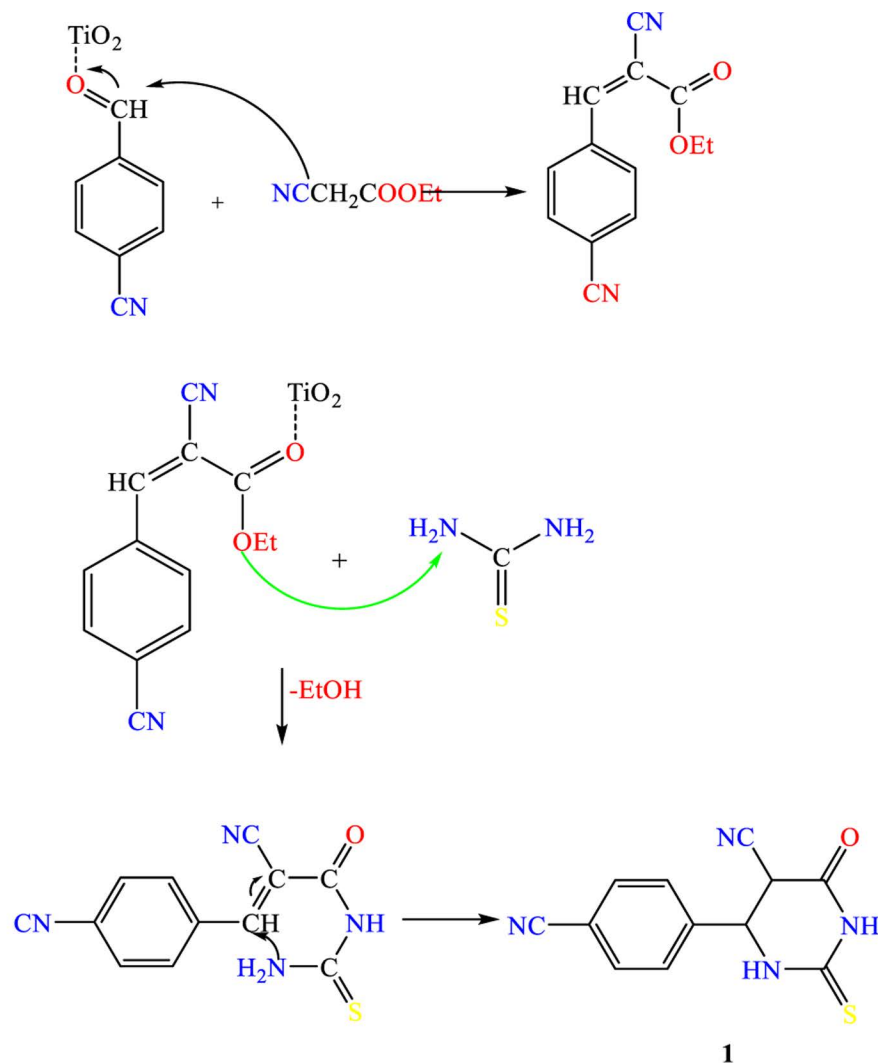
Scheme 1. Synthesis of 4-(4-cyanophenyl)-6-oxo-2-thioxohexahydropyrimidine-5-carbonitrile.

<https://doi.org/10.1371/journal.pone.0313959.g003>

of a C=S band at 1270 cm<sup>-1</sup>, an absorption band at 1721 cm<sup>-1</sup> which is due to the C=O group, an absorption band at 2224 cm<sup>-1</sup> due to the CN group, and an absorption band over the range cm<sup>-1</sup> attributed to the 2NH groups. Due to the CH aromatic, the <sup>1</sup>H NMR spectra show two doublet signals at 8.05 and 8.15. The spectra also show two singlet signals at 8.17 and 8.49 due to NH groups, whereas the <sup>13</sup>C NMR spectrum shows two signals at (δ in ppm) 115.06, 118.14 due to 2 CN groups, a signal at 161.22 due to C=O group and a signal due to C=S group at 183.81 (Scheme 2).

The introduction of a good leaving group was performed by treatment of (1) with methyl iodide in ethanolic sodium ethoxide, leading to the formation of the methyl-thio derivative (2). Also, the alkylation reaction is carried out using TiO<sub>2</sub>-NPs as an essential environment, while alkylation (cyanomethylation) with chloro-acetonitrile in ethanolic sodium ethoxide gave 2-((cyanomethyl)thio)-4-(4-cyanophenyl)-6-oxo-1,4,5,6-tetrahydropyrimidine-5-carbonitrile (3). Alkylation of Compound (1) with chloroacetone under primary conditions gave 4-(4-cyanophenyl)-6-oxo-2-((2-isopropyl)thio)-1,4,5,6-tetrahydropyrimidine-5-carbonitrile (4) (Scheme 3).

Treatment of (1) with acrylonitrile in pyridine gave 4-amino-8-(4-cyanophenyl)-6-oxo-7,8-dihydro-2H,6H-pyrimido[2,1-b][1,3]thiazine-7-carbonitrile (5). Compound (5) is also produced through the reaction of thiol Compound (1) by Cyanomethylation with acrylonitrile in the presence of TiO<sub>2</sub>-NPs as a catalytic amount in ethanol. The reaction of Compound (1) with ethyl chloroacetate under primary conditions gave the thiazolo[3,2-a]pyrimidine-6-carbonitrile derivative (6). In contrast, the reaction of Compound (1) with chloroacetic acid and benzaldehyde in the presence of sodium acetate under reflux in a mixture of glacial acetic acid and acetic anhydride gave the benzylidene derivative of thiazolo[3,2-a]pyrimidine-6-carbonitrile (7), (Scheme 4). The structures of Compounds (5), (6), and (7) were confirmed based on their spectral data (experimental part). A shred of evidence in confirmation of the structure of (2) is its conversion into 2-(benzo[d]thiazol-2-ylamino)-4-(4-cyanophenyl)-6-oxo-1,4,5,6-tetrahydropyrimidine-5-carbonitrile (8) by reaction with 2-amino benzothiazole in the presence of few drops of triethylamine and also its conversion

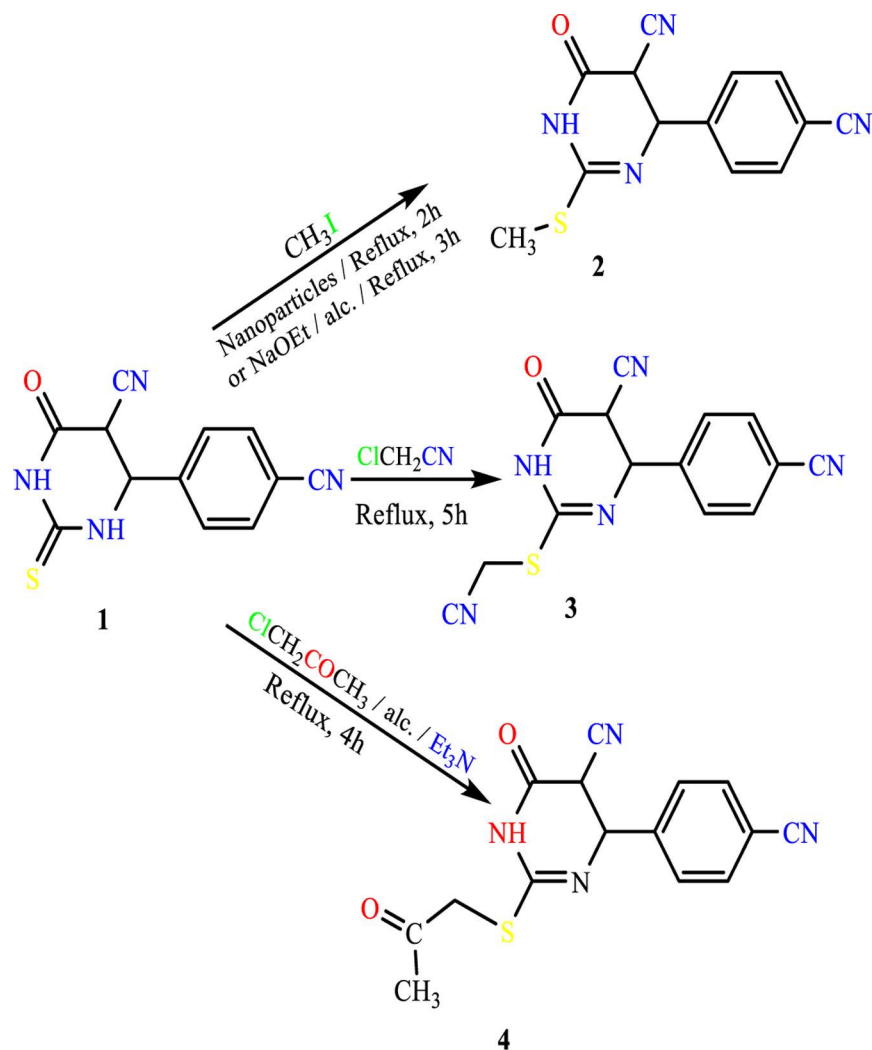


**Scheme 2: The possible mechanism for the synthesis of 4-(4-cyanophenyl)-6-oxo-2-thioxohexahydropyrimidine-5-carbonitrile (1)**

Scheme 2. The possible mechanism of the synthesis of 4-(4-cyanophenyl)-6-oxo-2-thioxohexahydropyrimidine-5-carbonitrile (1).

<https://doi.org/10.1371/journal.pone.0313959.g004>

into 4-(4-cyanophenyl)-6-oxo-2-(2-phenylhydrazine)-1,4,5,6-tetrahydropyrimidine-5-carbonitrile (**9**) by reaction with phenyl-hydrazine under similar condition, (Scheme 5). <sup>1</sup>H NMR spectra indicate the disappearance of the signal of the S-CH<sub>3</sub> methyl group of Compound **2** at  $\delta$  2.53 ppm. Compound **2** was obtained by reaction of 2-amino benzothiazole with a few drops of triethylamine afforded 2-(benzo[d]thiazol-2-ylamino)-4-(4-cyanophenyl)-6-oxo-1,4,5,6-tetrahydropyrimidine-5-carbonitrile (**8**). Under similar experimental conditions, Compound (**2**) was reacted with phenyl-hydrazine to yield 4-(4-cyanophenyl)-6-oxo-2-(2-phenylhydrazine)-1,4,5,6-tetrahydropyrimidine-5-carbonitrile (**9**) (Scheme 5).



**Scheme 3: Synthesis of S-alkylated pyrimidine derivatives.**

Scheme 3. Synthesis of S-alkylated pyrimidine derivatives.

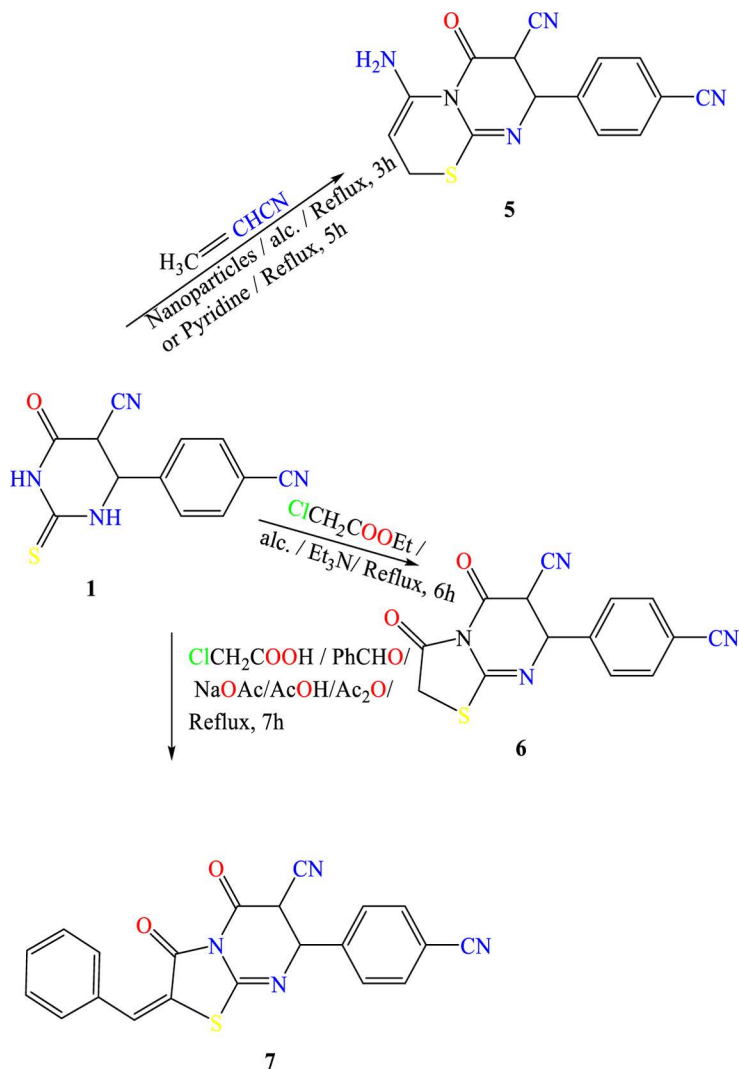
<https://doi.org/10.1371/journal.pone.0313959.g005>

## 2.3 Biology

**2.3.a Antioxidant activity.** The antioxidant activity of the newly synthesized compounds was evaluated using DPPH (2, 2-diphenyl-1-picrylhydrazyl (DPPH) assay). This assay measures the ability of a compound to neutralize the stable free radical DPPH by donating an electron or hydrogen atom. The results are illustrated in Table 2 and Fig 3. All the tests and analyses were undertaken in three replicates, and the results were averaged. All the tested compounds exhibited antioxidant activity. Compounds (5), (8), and (2) showed high activity with IC<sub>50</sub> 5.62, 6.21, and 10.09 µg/ml compared to 4.63 of standard ascorbic acid. Compounds (1), (4), and (3) showed moderate activity with IC<sub>50</sub> 25.13, 35.31, and 35.9, respectively.

The mechanism of antioxidant activity may be explained by inhibiting lipid peroxidation in addition to cyclooxygenase and lipo-oxygenase catalysis [29]. Also, previous studies [30,31]



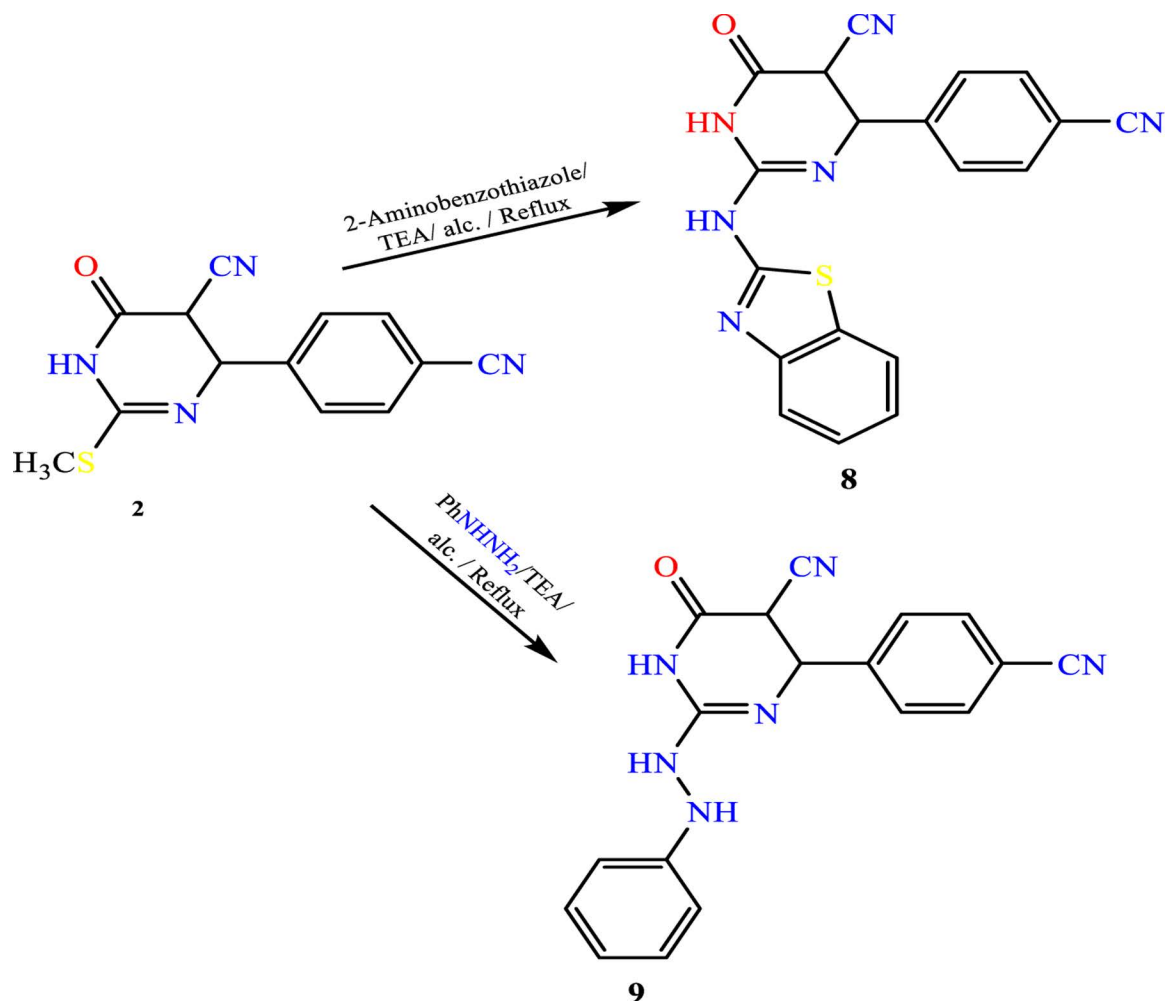


#### Scheme 4: Synthesis of fused pyrimidine derivatives

Scheme 4. Synthesis of fused pyrimidine derivatives.

<https://doi.org/10.1371/journal.pone.0313959.g006>

report that pyrimidine derivatives show antioxidant activity by DPPH scavenging ability. In addition, the incorporation of titanium dioxide nano-catalysts in synthesizing pyrimidine carbonitrile derivatives plays a crucial role in enhancing the antioxidant activity of the newly synthesized compounds. Titanium dioxide nano-catalysts can act as free radical scavengers and facilitate the regeneration of antioxidant compounds. It also modulates the cellular signaling pathway involved in oxidative stress and inflammation by enhancing superoxide dismutase, catalase, and glutathione peroxidase. Adding titanium dioxide nano-catalyst may enhance *in vivo* antioxidant activity through suppression of genes involved in apoptosis and immune response as NF- $\kappa$ B, FGFR2, and Casp8 and boosting pentose-phosphate, cysteine methionine, glycine-serine metabolism pathway [32].



### Scheme 5: Synthesis of isolated pyrimidine derivatives

Scheme 5. Synthesis of isolated pyrimidine derivatives.

<https://doi.org/10.1371/journal.pone.0313959.g007>

Table 2. Antioxidant activity of the synthesized compounds by using DPPH scavenging%.

Compound	IC <sub>50</sub> $\mu$ g/ml	Molecular wt(g/mol)	IC <sub>50</sub> $\mu$ M
Ascorbic acid	4.63	176.12	26.289
1	25.13	256.28	98.06
2	10.09	270.06	37.03
3	35.9	295.32	121.56
4	35.31	312.35	113.05
5	5.62	309.35	18.17
6	46.69	296.30	173.37
8	6.21	372.08	16.69
9	212.28	330.35	642.59

<https://doi.org/10.1371/journal.pone.0313959.t002>



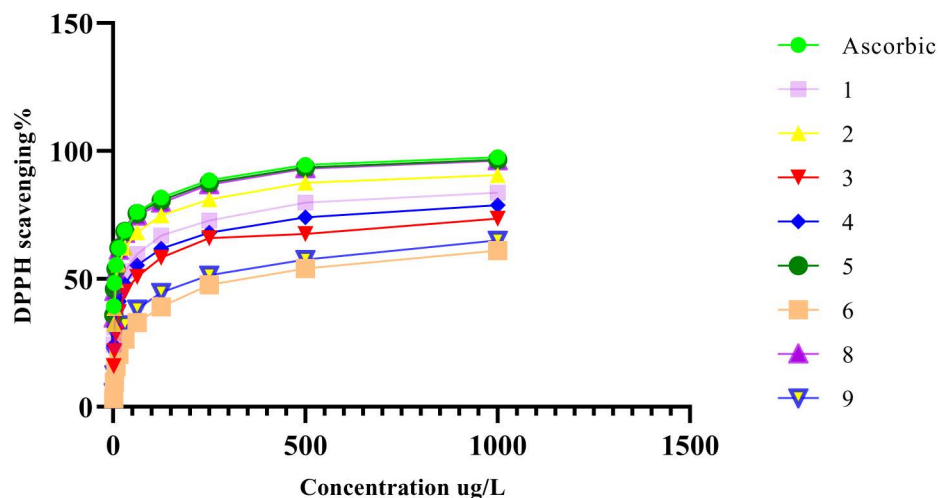


Fig 3. Antioxidant activity by DPPH radical scavenging method.

<https://doi.org/10.1371/journal.pone.0313959.g008>

Table 3. Anti-inflammatory activity by hemolysis.

Conc. ug/ml	Ab. Mean of Sample with RBCs	Sample with Isotonic solution Ab.	Hemolysis %	SD.
Control Complete Hemolysis	1.693	0.002	100	0.002
<b>Compound 1</b>				
1000	0.417	0.181	13.9	0.004
800	0.358	0.134	13.2	0.003
600	0.302	0.092	12.4	0.003
400	0.269	0.065	12.0	0.006
200	0.195	0.035	9.5	0.003
100	0.144	0.018	7.5	0.005
0	0.000	0.001	0.0	0.001
<b>Compound 2</b>				
1000	0.657	0.62	2.2	0.008
800	0.579	0.574	0.3	0.010
600	0.421	0.416	0.3	0.001
400	0.343	0.341	0.1	0.001
200	0.280	0.278	0.1	0.002
100	0.147	0.147	0.0	0.003
0	0.000	0.001	0.0	0.001
<b>Compound 3</b>				
1000	1.693	0.002	100	0.002
800	0.348	0.309	2.3	0.004
600	0.239	0.218	1.2	0.003
400	0.173	0.161	0.7	0.002
200	0.091	0.085	0.3	0.002
100	0.044	0.043	0.1	0.002
0	0.029	0.027	0.1	0.001
<b>Compound 4</b>				
1000	0.281	0.123	9.3	0.002
800	0.218	0.087	7.8	0.002

(Continued)

Table 3. (Continued)

Conc. ug/ml	Ab. Mean of Sample with RBCs	Sample with Isotonic solution Ab.	Hemolysis %	SD.
600	0.161	0.062	5.9	0.006
400	0.102	0.041	3.6	0.003
200	0.055	0.024	1.8	0.002
100	0.034	0.011	1.3	0.002
0	0.000	0.001	0.0	0.001
<b>Compound 5</b>				
1000	0.462	0.344	7.0	0.009
800	0.378	0.278	5.9	0.003
600	0.328	0.235	5.5	0.005
400	0.265	0.241	1.4	0.002
200	0.156	0.15	0.4	0.002
100	0.101	0.098	0.2	0.005
0	0.000	0.001	0.0	0.001
<b>Compound 6</b>				
1000	0.367	0.125	14.3	0.002
800	0.312	0.095	12.8	0.003
600	0.148	0.071	4.6	0.111
400	0.109	0.041	4.0	0.002
200	0.084	0.032	3.1	0.002
100	0.060	0.025	2.1	0.005
0	0.000	0.001	0.0	0.001
<b>Compound 8</b>				
1000	0.638	0.575	3.7	0.020
800	0.444	0.394	3.0	0.003
600	0.300	0.278	1.3	0.002
400	0.185	0.169	0.9	0.004
200	0.117	0.115	0.1	0.002
100	0.093	0.093	0.0	0.002
0	0.000	0.001	0.0	0.001
<b>Compound 9</b>				
1000	0.485	0.241	14.4	0.007
800	0.302	0.133	10.0	0.004
600	0.244	0.092	9.0	0.001
400	0.149	0.064	5.0	0.003
200	0.117	0.045	4.3	0.002
100	0.070	0.022	2.9	0.002
0	0.000	0.001	0.0	0.001

<https://doi.org/10.1371/journal.pone.0313959.t003>

**2.3.b Anti-inflammatory activity.** The hemolysis assay of the synthesized compounds is summarized in Table 3 and Fig 4; the mean absorption rate of the samples, with isotonic solution Ab, and hemolysis % were calculated with a standard deviation. HRBC and membrane stabilization assay results provide valuable information about the potential anti-inflammatory effects of the newly synthesized pyrimidine carbonitrile derivatives. All the tested compounds showed potent anti-inflammatory activity. The most powerful compounds were (2) and (8), as there was no hemolysis when rheu was used at 100 µg/ml, followed by Compound (5),

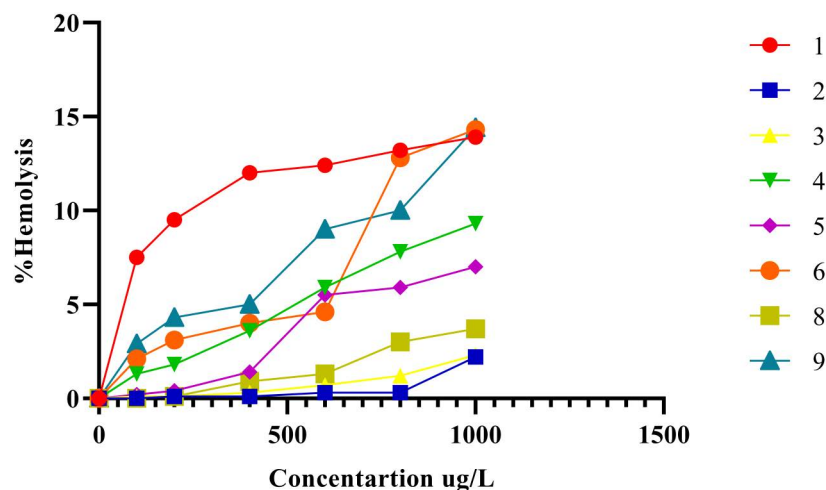


Fig 4. Anti-inflammatory activity of the tested compounds.

<https://doi.org/10.1371/journal.pone.0313959.g009>

which exhibited 0.2% hemolysis when used at the same concentration. The results for the anti-inflammatory activity are in agreement and homogenous with those obtained from the antioxidant activity of the same compounds, as shown in Table 3. The interconnection between inflammation and oxidative stress plays a vital role in the induction of several chronic diseases, such as diabetes, rheumatoid arthritis, and inflammatory bowel disease—inflammation results in the release of inflammatory mediators and, subsequently, tissue damage. Oxidative stress occurs due to an imbalance between the production of the reactive oxygen species and the ability of the body to neutralize them. Several cellular mechanisms are involved in the anti-inflammatory activity of the tested compounds. A previous study [33] reports that pyrimidine, as a heterocyclic compound, shows potent anti-inflammatory activity in carrageenan-induced rat paw edema by inhibiting the inflammatory mediator PGE 2 via the inhibitory activity of cyclooxygenase enzymes. The cellular mechanism of action was detected by suppression of myeloperoxidase and granulocyte superoxide formation. These compounds also inhibit the expression of TNE, nuclear factor  $\kappa$ B, interleukins, and leukotrienes. Another *in vivo* study [34] explains that some pyrimidine derivatives possess anti-inflammatory activity greater than both standard celecoxib and diclofenac sodium in both formalin-induced paw edema and cotton pellet granuloma in rats in acute and chronic inflammation models. In addition, other mechanisms may explain the anti-inflammatory activity through the inhibitory effect on nitric acid synthase and lipo-oxygenase enzymes [35,36].

## 2.4 In-silico-studies

### 2.4.a Molecular docking.

**2.4.a.1 Anti-inflammatory activity** To acquire insights into the underlying mechanisms of action of the newly synthesized pyrimidine carbonitrile derivatives, we carried out virtual docking of the highly selective COX-2 inhibitors with Compounds 5 and 8 within the active binding site of the COX-2 enzyme. The co-crystal structure of the COX-2 complex with SC-558, a selective COX-2 blocker, was acquired from the PDB (protein data bank) PDB: 1CX2. Fig 5 indicates the 2D and 3D snap of the interacting compounds with receptors. The docked co-crystal is used for validation and shows docking score energy with -7.23 kcal/mole with rmsd of 1.556, the docked co-crystal and the PDB 1CX2 showed interaction at ARG 469 (A) H-donor, SER 471 (A) H-acceptor, and GLN 543 (B) pi-H. The docked complexes 5 and 8 showed docking score energy expressed in kcal/mol with -6.45, and -7.4099, with rmsd values 0.8358 and



**2.4.a.2. Antioxidant activity** A molecular docking study of the newly synthesized pyrimidine carbonitrile derivatives was carried out on Compounds (5) and (8) using co-crystallized ascorbic acid as a reference ligand, isolated from cytochrome c peroxidase enzyme PDB: 2X08. The docked co-crystal is used for validation and shows docking score energy with -4.93 kcal/mole with rmsd of 0.564, the docked co-crystal and the PDB 2X08 showed interaction at LYS 179 (A), with H- donor, ARG 48 (A) H-acceptor, and ARG 184 (A) H-acceptor. The docked complexes 5 and 8 showed docking score energy with -7.005, and -7.89, with rmsd values 1.21 and 1.29 respectively. The results are represented in Fig 6, indicating the 2D and 3D snap of the interactive compounds with receptors.. Docked complex 5 showed interactions with HIS 175 (A) H-acceptor, HIS 175 (A) pi-pi, TRP 51 (A) pi-pi, and Arg84 by ligand exposure with binding to the  $\gamma$ -heme edge of cytochrome c peroxidase. Docked complex 8 showed interactions at LYS 179 (A) H-donor, LYS 179 (A) H-acceptor, and HIS 181 (A) pi-H. at the same time, the docked co-crystal showed interactions at LYS 179 (A) H-donor, ARG 48 (A) H-acceptor, and ARG 184 (A) H-acceptor.

#### 2.4.b Pharmacokinetics.

**ProTox-II** ProtoxII virtual lab is used to predict the toxicities of small molecules.

Predicting compound toxicities is an integral part of the drug design development process. The ProTox-II shows that the four compounds are expected to have oral LD50 values ranging from 159 to 2480 mg/kg in a rat model with (1 s,4s)-eucalyptol having the highest values and quercetin the lowest. The toxicity radar Fig 7 is intended to quickly illustrate the confidence of positive toxicity results compared to the average of its class for Compounds (5) and (8) (Table 4).

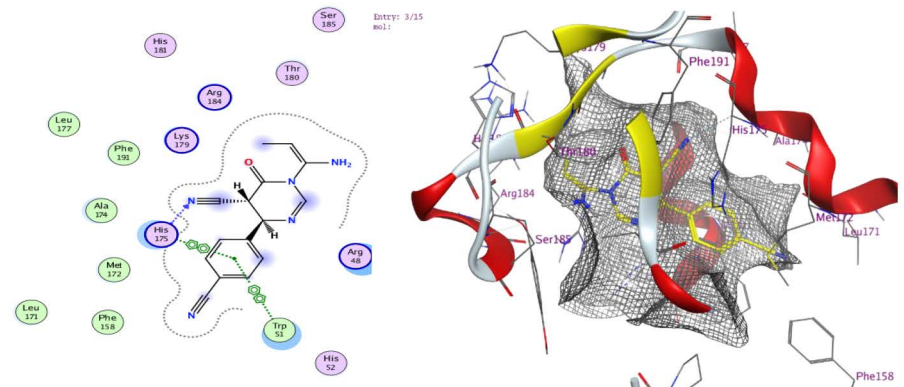
**Pred-hERG** Chemically similar compounds can have different effects on different protein targets, and proteins may not always be able to distinguish between similar ligands. To improve machine learning predictions, knowledge of pharmacological and off-target relationships between proteins and the similarity of ligand sets can be used to interpolate outputs and ensure that predictions are consistent with compound similarity criteria. This pipeline helps to improve the forecasts of off-target drug effects and reduce the false-negative error. Chemical similarity is one of the essential concepts in cheminformatics. One commonly used to calculate these similarity algorithm measures is the 2D Tanimoto algorithm employed here. The resulting Tanimoto coefficient is fingerprint-based, encoding each molecule to a fingerprint “bit” position (MACCS), with each bit recording the presence (“1”) or absence (“0”) of a fragment of the molecule. The potency results are represented in Table 5b, while Fig 8 shows the probability mp of Compounds (5) and (8). The similar off-compounds of Compounds (5) and (8) are represented in Fig 9 and Fig 10.

**Similar off-compounds induced by labMol for Molinspiration** The predicted pharmacokinetic/Molinspiration properties of the pyrimidine carbonitrile derivatives (5) and (8) are given in Table 5a. With the help of Molinspiration virtual screening, most synthesized compounds showed promising bioactivity as implied by docking parameters in Table 5b, which indicates the drug-likeness properties against kinase inhibitors, protease, and enzyme inhibitors. The calculated distribution of activity scores (version 2011.06), GPCR ligands, kinase inhibitors, ion channel modulators, nuclear receptor ligands, protease inhibitors, and other enzyme targets are compared with scores for about 100,000 average drug-like molecules. The score allows efficient separation of active and inactive molecules.

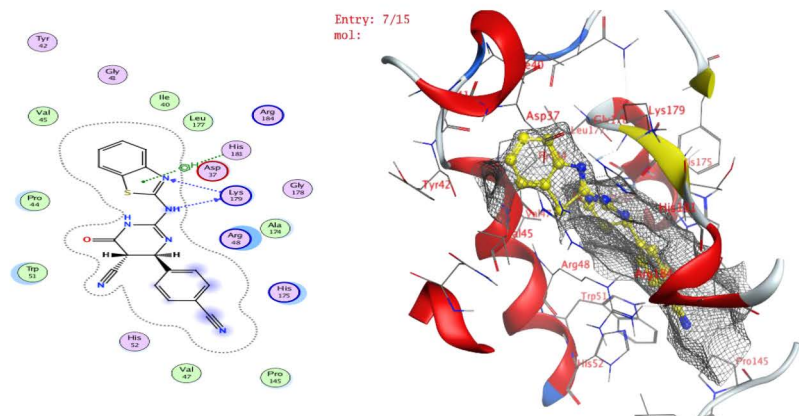
**2.4.c. DFT.** Density functional theory (DFT) based quantum chemical calculations were carried out for compounds 5 and 8 to demonstrate their relative reactivity as an anti-inflammatory and antioxidant. The frontier molecular orbital pictures of 5 and 8 and their corresponding reactivity parameters are presented in Fig 11 and Table 6, respectively. The DFT/ B3LYP approach was used in the current study to perform quantum chemical computations to optimize the selected structures. The DFT (B3LYP) method with 6-311G++(d,p) basis



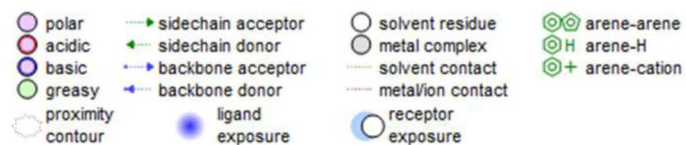
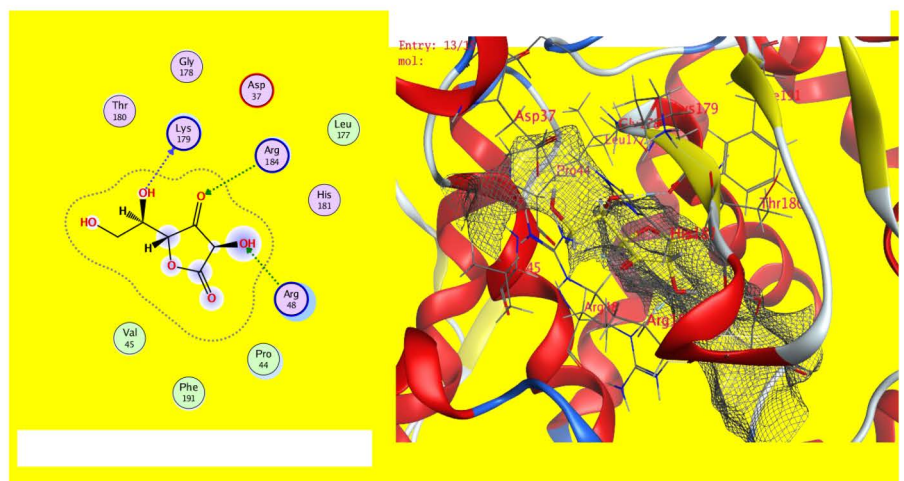
5



8



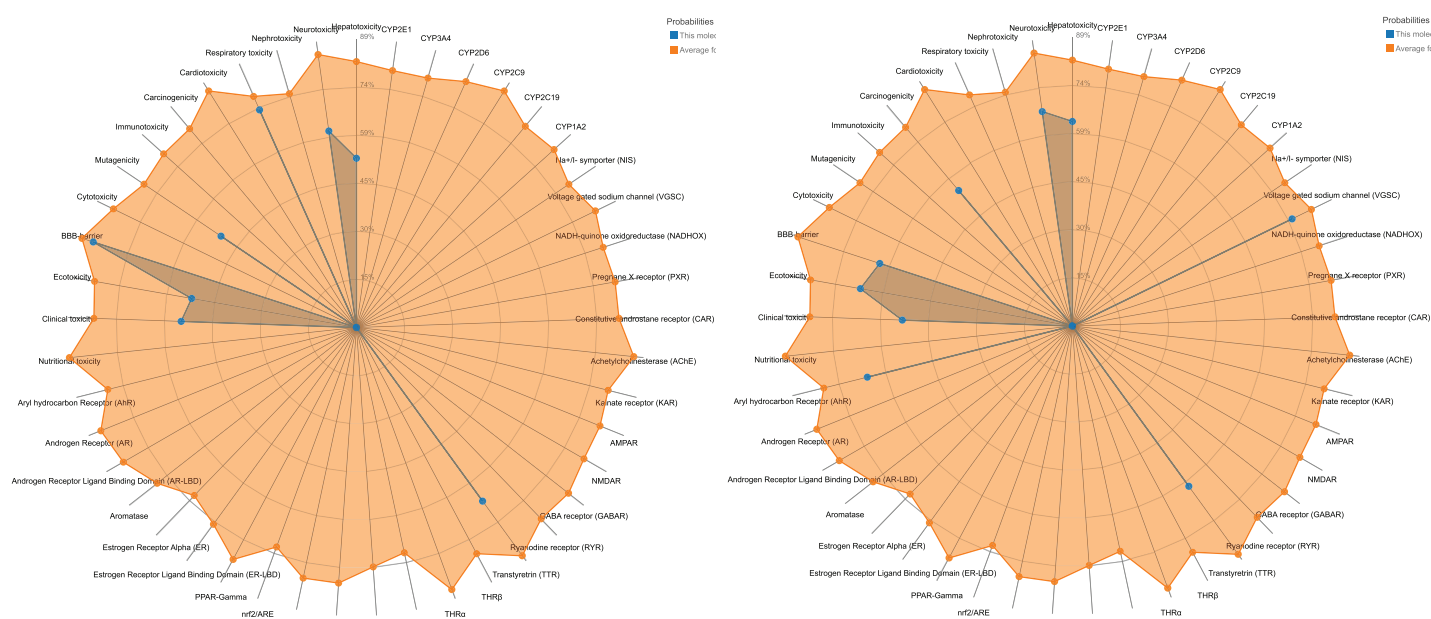
Co-crystal validation

Fig 6. The interaction of *c* peroxidase enzyme PDB: 2X08.
<https://doi.org/10.1371/journal.pone.0313959.g011>

**Table 4.** The predicted toxicity for (5) and (8) using (a) the ProTox-II and (b) the Pred-HERG software.

	5	8
<b>a-Pro-ToxII</b>		
Predicted LD50 (mg/kg)	700 mg/kg	1000 mg/kg
Predicted toxicity class	4	
Average similarity (%)	54.72%	54.01%
Prediction accuracy (%)	67.38%	67.38%
<b>b-Pred-HERG</b>		
Prediction/Potency	Weak or Moderate	Weak or Moderate
Confidence (%)	60	60
Applicability domain (AD.)	No (Value = 0.25 and limit = 0.26)	No (Value = 0.28 and limit = 0.26)

<https://doi.org/10.1371/journal.pone.0313959.t004>

**Fig 7.** The toxicity radar chart is intended to quickly illustrate the confidence of positive toxicity results compared to the average of its class for Compounds (5) and (8).

<https://doi.org/10.1371/journal.pone.0313959.g012>

set was applied in this test. The electrostatic potential map, the optimized structure, and its HOMO and LUMO values are represented in Fig 12 HOMO energy expresses the ability of the compound to act as an electron donor. On the other hand, a site's LUMO energy can act as an electron attractor. The electrostatic potential maps of the compounds show areas with electron localization throughout the molecules, with red and blue colors representing electron-rich (negative) and deficient (favorable) locations, respectively. Finally, Table 6 describes the DFT calculations that reveal favorable energetic parameters ( $E_{\text{HOMO}}$ ,  $E_{\text{LUMO}}$ ,  $\Delta E$ , Ionization Energy IE, and Electron affinity EA) for the selected Compounds 5 and 8.



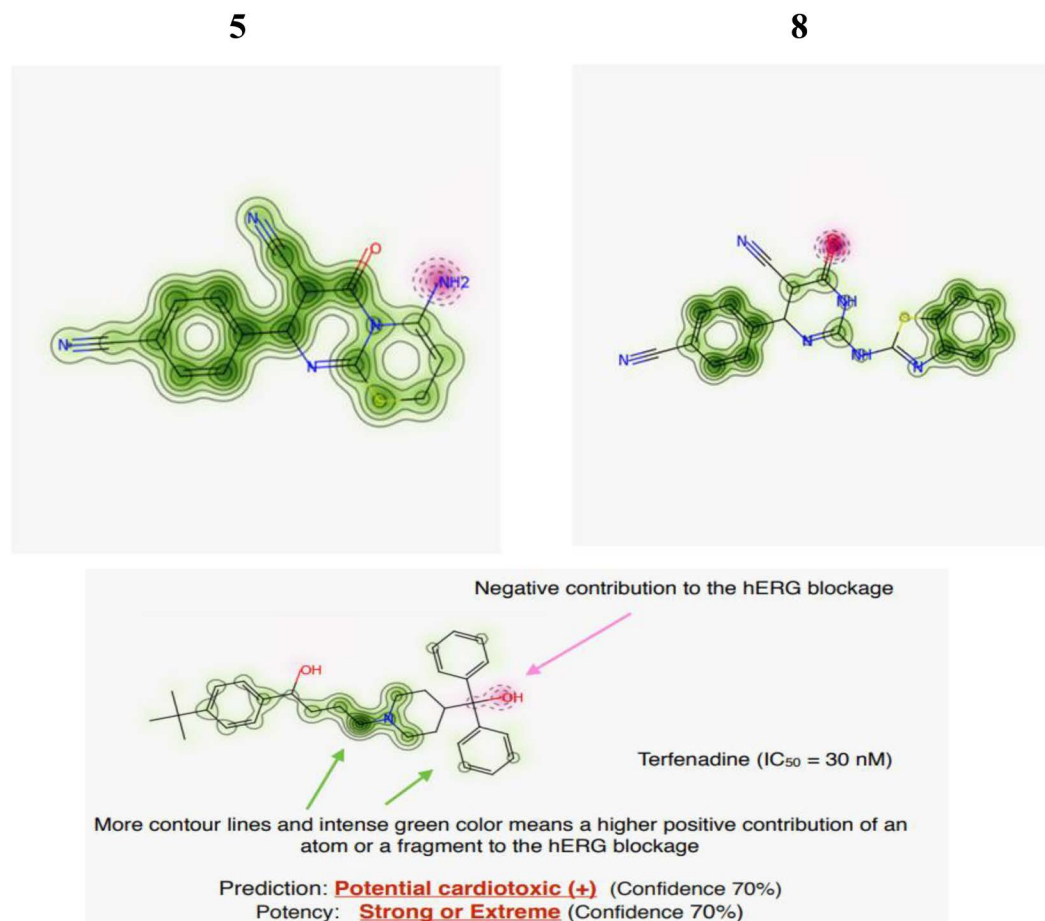


**Fig 8.** Pred-hERG results. Probability map of Compounds (5) and (8).

<https://doi.org/10.1371/journal.pone.0313959.g013>

### 3. Experimental

#### 3.1. Materials and methods

High-grade materials were used to synthesize the target compounds. Chemicals were obtained from Sigma-Aldrich (Taufkirchen, Germany). Sigma-Aldrich Company provided solvents. The manufactured Mn<sub>3</sub>O<sub>4</sub> nanoparticles were provided by the National Research Centre (NRC) by means of precipitation technique chemicals (ethyl cyanoacetate 99%, thiourea 99.5% and 4-cyanobenzaldehyde 99%, methyl iodide, chloroacetone, chloro-acetonitrile, acrylonitrile, ethyl chloroacetate, 2-amino benzothiazole, phenyl-hydrazine) were obtained from Sigma-Aldrich (Taufkirchen, Germany). Titanium (IV)isopropoxide (97%) was obtained from Merck Co. Solvents (ethanol 99.8%, pyridine, acetic anhydride, and acetic acid 99.7%) were provided by Sigma Aldrich Company. The National Research Center (...) provided TiO<sub>2</sub> nanoparticles. The transmission Electron Microscope (TEM) sample was loaded on a carbon-coated Cu grid (200 mesh) and inspected at 200 kV utilizing JEM-2100 (JEOL, Tokyo, Japan)—electron microscopy unit- National Research Centre. The National Research Center screened the X-ray diffraction (XRD) pattern with the D8 Advance diffractometer (Bruker, Germany). Quantachrome Touch WinTM, model NOVA touch 4LX, measured specific surface area (SSA). The melting points were uncorrected and were measured by a digital Electrothermal IA 9100 Series apparatus

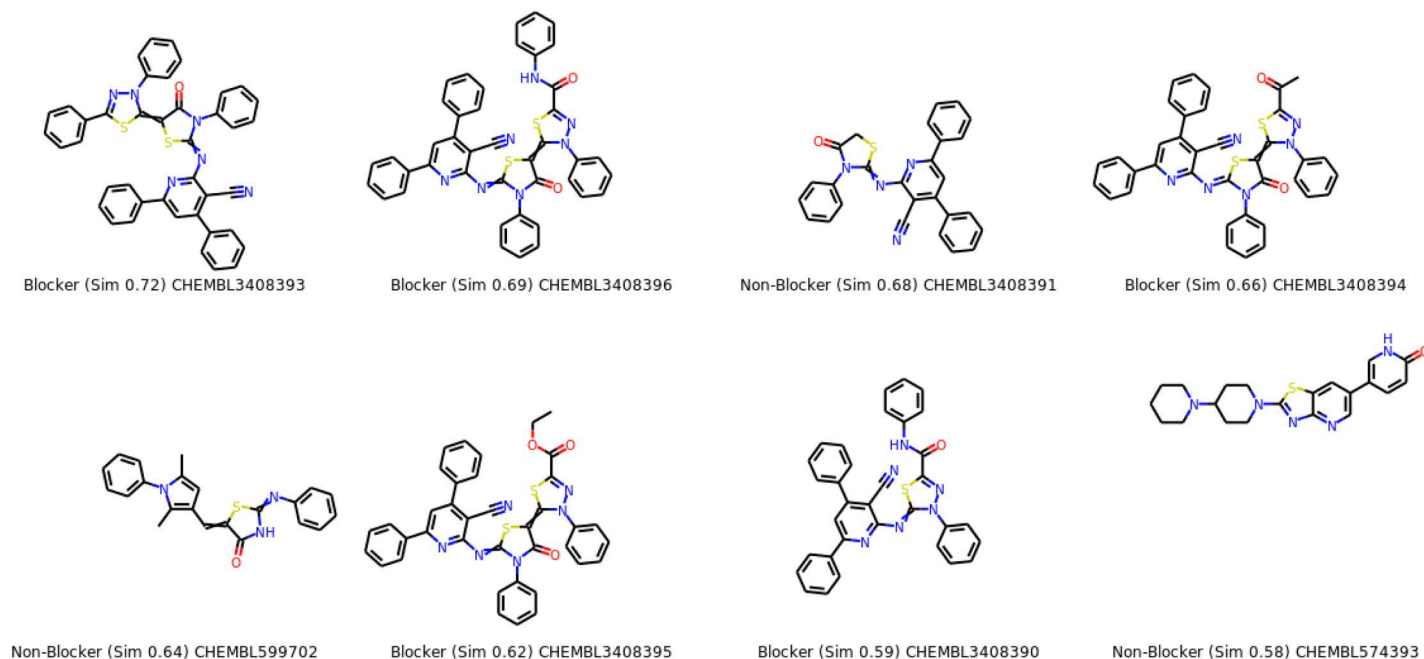


Fig 9. compound 5.

<https://doi.org/10.1371/journal.pone.0313959.g014>

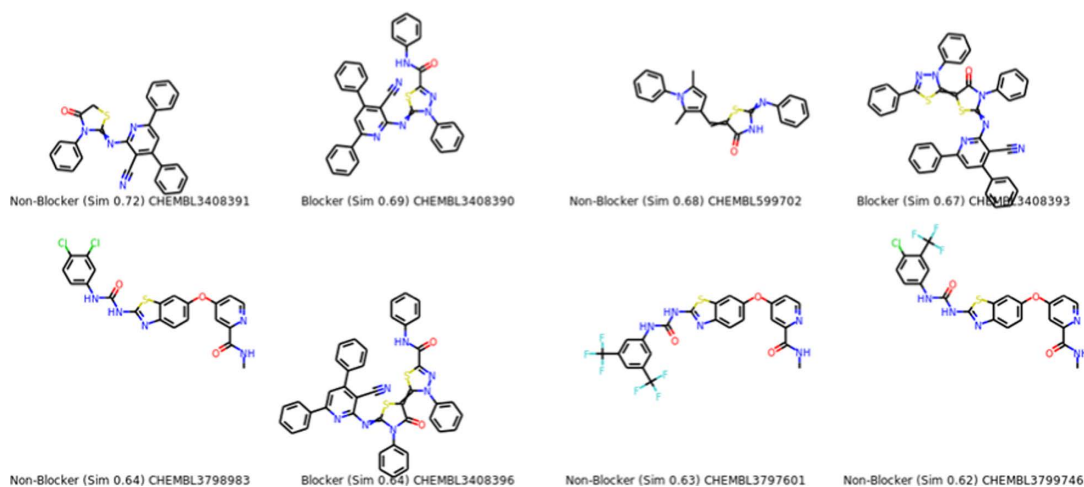


Fig 10. compound 8.

<https://doi.org/10.1371/journal.pone.0313959.g015>

Cole-Parmer, UK). A PerkinElmer CHN 2400 was utilized for C, H, and N analyses. IR spectra were obtained from 4000 to 400 cm<sup>-1</sup> using FT-IR 460 PLUS (KBr disks). A Bruker 800 MHz NMR spectrometer was used for recording <sup>1</sup>H and <sup>13</sup>C-NMR spectra, the solvent utilized was DMSO-d<sub>6</sub>, and chemical shifts were obtained at KAUST and stated in δ (ppm). Cytotoxicity on Vero cell [HAV] was performed at the Pharmacology Department, Faculty of Veterinary Medicine, Cairo University, Cairo, Egypt.

Table 5. Physicochemical properties of the synthesized compounds.

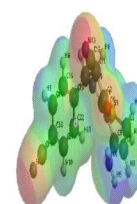
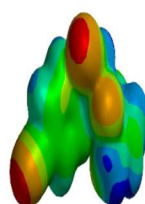
Compound	miLogP	TPSA	n-atoms	MW.	nON	nOHNH	n-violations	n-rotb	Volume
5	0.31	106.28	22	309.35	6	2	0	1	258.40
8	2.72	113.97	27	372.41	7	2	0	0	309.58

## b-Physicochemical Molinspiration bioactivity score

Compound	GPCR ligand	Ion channel modulator	Kinase inhibitor	Nuclear receptor ligand	Protease inhibitor	Enzyme inhibitor
5	-0.51	-0.72	-0.81	-0.99	-0.35	-0.44
8	-0.29	-0.44	-0.42	-0.81	-0.26	-0.29

<https://doi.org/10.1371/journal.pone.0313959.t005>

5



8

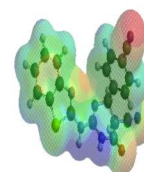
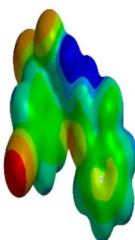


Fig 11. Electrostatic potential map of Compounds (5) and (8).

<https://doi.org/10.1371/journal.pone.0313959.g016>

Table 6. DFT-based reactivity parameters for compounds 5 and 8 derived using the Spartan 20 software package and the B3LYP/ 6-31 G (d,p) system.

S/N	E <sub>HOMO</sub>	E <sub>LUMO</sub>	ΔE	IE	EA
5	-6.02	0.72	5.3	6.02	-0.72
8	-9.06	-0.67	8.39	9.06	0.67

<https://doi.org/10.1371/journal.pone.0313959.t006>

### 3.2. Preparation of TiO<sub>2</sub>

Titania (TiO<sub>2</sub>) powders retain remarkable optical, dielectric, and catalytic properties, which point to industrial applications. The titanium (IV) isopropoxide hydrolysis process prepared the titanium dioxide nanoparticles. The preparatory solution was a combination of titanium (IV) isopropoxide, 98% (TTIP, ACROS organics, MW = 284.26), and isopropanol (CH<sub>3</sub>CHOHCH<sub>3</sub>). An appropriate volume of TTIP was dissolved in the proper amount of isopropanol (99.5%). A solution of distilled water with a pH value of 2 was used as a hydrolysis medium, and the pH was adjusted by adding nitric acid (HNO<sub>3</sub>). A pale yellow solution was produced when mixed under



vigorous stirring. The resulting pale-yellow unclear solution was heated to 60–70°C for 18–20 h. The solution was kept under stirring until its volume decreased, and a refined suspension was produced. The yellowish-white suspension was dried at 100°C for 6 h.

### 3.3. XRD

The formed phase of TiO<sub>2</sub> was recognized from the X-ray diffraction (XRD) patterns inspected by the D8 Advance diffractometer (Bruker, Germany). The diffractogram was in terms of 2θ in the range of 10–80°. The JCPDS-International Center for Diffraction Data Cards was used as a reference for the documentation of the formed phases.

### 3.4. TEM

Particle size was confirmed by transmission electron microscopy (TEM; JEOL, Japan, JEM 2100, Electron Microscope, TEM-HR). First, particles were dispersed in ethanol, then a few milliliters of the solution were dropped onto a copper grid, and a TEM image was obtained.

### 3.5. Specific Surface Area (SSA)

SSA is a material property; it plays a significant role in the formation of nanoparticles, owing to the large surface-to-volume ratio and particle size reduction. Therefore, it has a precise significance in adsorption, heterogeneous catalysis, and surface reactions. Furthermore, the high surface area of the TiO<sub>2</sub> nanoparticles enables the reaction/interaction between TiO<sub>2</sub> and the interacting media, which mainly occurs on the surface or at the interface and is intensely influenced by the material's surface area [37]. In the current study, Quantachrome TouchWin™, model NOVA Touch 4LX measured the surface area of the prepared TiO<sub>2</sub> at 169.339 (m<sup>2</sup>/gm).

### 3.6. Chemistry

#### 4-(4-cyanophenyl)-6-oxo-2-thioxohexahydropyrimidine-5-carbonitrile (1).

##### General procedure for (1) Traditional method

A mixture of ethyl cyanoacetate (1.13 g, 10 mmol), thiourea (0.76 g, 10 mmol), and 4-cyanobenzaldehyde (1.31 g, 10 mmol) in 10 ml ethanol and a few drops of triethylamine was heated under reflux for 3 h. The solid product obtained after cooling was filtered off, washed with ethanol, and recrystallized from ethanol to yield yellow crystals (yield: 35%) m.p. 167–170°C.

##### Nanocatalytic method

To a mixture of ethyl cyanoacetate (1.13 g, 10 mmol), thiourea (0.76 g, 10 mmol), and 4-cyanobenzaldehyde (1.31 g, 10 mmol) in 10 ml ethanol, nano TiO<sub>2</sub> (0.079 g, 1 mmol) was added. The reaction mixture was refluxed for 1 h, then filtered off on heat to remove the nanocatalyst. The reaction mixture was allowed to cool, and then the solid product obtained after cooling was filtered off, washed with ethanol, dried, and recrystallization from ethanol to afford yellow crystals (yield: 40%) m.p. 167–170 °C.

**4-(4-cyanophenyl)-6-oxo-2-thioxohexahydropyrimidine-5-carbonitrile (1).** IR (KBr, ν, cm<sup>-1</sup>): 3343–3521 cm<sup>-1</sup> (2NH str), 3153–2993 cm<sup>-1</sup> (CH for aromatic and aliphatic), 2224 cm<sup>-1</sup> (CN), 1721 cm<sup>-1</sup> (C=O), 1270 cm<sup>-1</sup> (C=S). <sup>1</sup>H-NMR (DMSO-d<sub>6</sub>, 500 MHz): δ = 3.34 (s, 1H, methine-CH-CN), 4.34 (d, 1H, CH(CN)-CH-Ar), 8.05, 8.15 (d, d, 4H, CH Aromatic), and 8.49 ppm (s, 2H, 2NH). <sup>13</sup>C-NMR (DMSO-d<sub>6</sub>, 500 MHz): δ = 39.5, 62.7, 106.09, 114.5, 115.06, 118.14, 131.001, 133.01, 135.5, 153.1, 161.2, 183.8 ppm. MS: m/e M<sup>+</sup> 256.8, M<sup>+</sup> 257.1, M-S atom 224.8. Anal. Calcd. for C<sub>12</sub>H<sub>8</sub>N<sub>4</sub>OS (256.28): C, 56.24; H, 3.15; N, 21.86; S, 12.51

**4-(4-Cyanophenyl)-2-(methylthio)-6-oxo-1,4,5,6-tetrahydro pyrimidine-5-carbonitrile (2).**

**Traditional method** A solution of Compound (1) (2.56 g, 10 mmol) and methyl iodide (1.4 g, 10 mmol) in ethanolic sodium ethoxide (0.23 g, 10 mmol/ 20 ml ethanol), the reaction mixture was refluxed for 3 h, then allowed to cool and poured into ice water. The solid product obtained after acidification with hydrochloric acid (6 ml, 30% soln.) was filtered off, washed with water, dried, and recrystallization from ethanol to afford a yellow powder (yield: 60%) m.p. 297–300°C.

**Nanocatalytic Method** To a solution of Compound (1) (2.56 g, 10 mmol) and methyl iodide (1.4 g, 10 mmol) in ethanol (10 ml), nano TiO<sub>2</sub> (0.079 g, 1 mmol) was added. The reaction mixture was refluxed for 2 h, then filtered off on heat to remove the nanocatalyst. The reaction mixture was allowed to cool, and then the solid product obtained after cooling was filtered off, washed with ethanol, dried, and recrystallization from ethanol to afford yellow crystals (yield: 72%) m.p. 297–300°C. IR (KBr,  $\nu$ , cm<sup>-1</sup>): 3490 (NH, str), 3083–2858 (CH for aromatic and aliphatic), 2231 (CN), 1663 (C=O). <sup>1</sup>H-NMR (DMSO-d<sub>6</sub>, 500 MHz):  $\delta$  = 2.53 (s, 3H, J =, CH<sub>3</sub>), 3.49 (s, 1H, J =, methine-CH-CN), 2.69 (d, 1H, J =, CH(CN)-CH-Ar), 8.05, 8.09 (d, d, 4H, CH Aromatic), and 13.943 ppm (s, 1H, NH). <sup>13</sup>C-NMR (DMSO-d<sub>6</sub>, 500 MHz):  $\delta$  = 13.39, 39.5, 40.41, 94.19, 113.88, 115.51, 118.25 (2CN), 129.53, 132.59, 139.61, 160.69, 165.72, 167.39 (C=O) ppm. Anal. Calcd. for C<sub>13</sub>H<sub>10</sub>N<sub>4</sub>OS (270.06): C, 57.76; H, 3.73; N, 20.73; S, 11.86

**2-((Cyanomethyl)thio)-4-(4-cyanophenyl)-6-oxo-1,4,5,6-tetrahydropyrimidine-5-carbonitrile (3).** A solution of Compound (1) (0.256 g, 1 mmol) in ethanolic sodium ethoxide (0.0345 g, 1.5 mmol/ 5 ml ethanol) was stirred at room temperature for 1 h, chloro-acetonitrile (0.09 g, 1.2 mmol) was added to the reaction mixture, followed by gentle heating for 5 h, then allowed to cool and poured into ice water. The solid product obtained after acidification with hydrochloric acid (6 ml, 30% soln.) was filtered off, washed with water, dried, and recrystallization from ethanol to afford a dark brown powder (yield: 80%) m.p. over 300°C. IR (KBr,  $\nu$ , cm<sup>-1</sup>): 3450 (NH, str), 2235, 2204 (2CN), 1642 (C=O). <sup>1</sup>H-NMR (DMSO-d<sub>6</sub>, 500 MHz):  $\delta$  = 3.61 (s, 1H, J =, (methine-CH-CN), 2.49 (d, 1H, J =, CH(CN)-CH (Ar), 4.16 (s, 2H, -S-CH<sub>2</sub>-CN), 7.914, 7.931 (d, 4H, CH Aromatic), and 8.06 (s, 1H, NH) ppm. Anal. Calcd. for C<sub>14</sub>H<sub>9</sub>N<sub>5</sub>OS (295.32): C, 56.94; H, 3.07; N, 23.71; S, 10.86.

**4-(4-Cyanophenyl)-6-oxo-2-((2-oxo-propyl)thio)-1,4,5,6-tetrahydro-pyrimidine-5-carbonitrile (4).** A mixture of Compound (1) (0.256 g, 1 mmol) and chloroacetone (0.11 g, 1.2 mmol) in ethanol (5 ml) and a few drops of triethylamine was allowed to reflux for 4 h; after that, the reaction mixture was cooled. The precipitated solid product was filtered off, washed with ethanol, dried, and recrystallized from ethanol to yield a pale brown powder (yield: 65%) m.p. over 300°C. IR (KBr,  $\nu$ , cm<sup>-1</sup>): 3427 (NH, str), 3065–2971 (CH for aromatic and aliphatic), 2228 (CN), 1738, 1664 (2 C=O). <sup>1</sup>H-NMR (DMSO-d<sub>6</sub>, 500 MHz):  $\delta$  = 2.2 (s, 3H, J =, CO-CH<sub>3</sub>), 4.16 (s, 2H, J =, S-CH<sub>2</sub>-CO), 3.33 (d, 1H, CH(CN)-CH(Ar), 5.297 (s, 1H, methine-CH-CN), 8.087, 8.100 (d, 4H, Aromatic) ppm. Anal. Calcd. for C<sub>15</sub>H<sub>12</sub>N<sub>4</sub>O<sub>2</sub>S (312.35): C, 57.68; H, 3.87; N, 17.94; S, 10.26

**4-Amino-8-(4-cyanophenyl)-6-oxo-7,8-dihydro-2H,6H-pyrimido[2,1-b][1,3]thiazine-7-carbonitrile (5).**

**Traditional method** To a solution of Compound (1) (2.56 g, 10 mmol) in (20 ml) pyridine, acrylonitrile (0.53 g, 10 mmol) was added, and the reaction mixture was refluxed for 5 h. After cooling at room temperature, the reaction mixture was poured into ice water. The solid product was obtained after acidification with hydrochloric acid (6 ml, 30% soln.), filtered off, washed with water, dried, and recrystallized from ethanol to afford a yellow powder (yield: 45%) m.p. 240–245°C. F

**Nanocatalytic method** To a solution of Compound (1) (0.256 g, 1 mmol) and acrylonitrile (0.053 g, 1 mmol) in ethanol (5 ml), nano TiO<sub>2</sub> (0.008 g, 10 mmol) was added. The reaction mixture was refluxed for 3 h, then filtered off on heat to remove the nanocatalyst.



The reaction mixture was allowed to cool, and then the solid product obtained after cooling was filtered off, washed with ethanol, dried, and recrystallization from ethanol to yield yellow crystals (yield: 57%) m.p. 240–245°. (yield: 45–70%) m.p. 240–245°C. IR (KBr,  $\nu$ ,  $\text{cm}^{-1}$ ): 3157–3491 ( $\text{NH}_2$ , str), 3085–2870 (CH for aromatic and aliphatic), 2230 (CN), 1678 (C=O). <sup>1</sup>H-NMR (DMSO- $d_6$ , 500 MHz):  $\delta$  = 2.49 (d, 1H, CH(CN)-CH(Ar), 3.1 (s, 1H, methine-CH(CN)), 3.64 (d, 2H, S-CH<sub>2</sub>-CH) 4.3 (t, 1H, S-CH<sub>2</sub>CH), 7.85, 7.86 (d, 4H, Aromatic), and 8.9 (s, 2H,  $\text{NH}_2$ ) ppm. Anal. Calcd. for  $\text{C}_{15}\text{H}_{11}\text{N}_5\text{OS}$  (309.35): C, 58.24; H, 3.58; N, 22.64; S, 10.36.

**7-(4-Cyanophenyl)-3,5-dioxo-2,3,6,7-tetrahydro-5H-thiazolo[3,2-a]pyrimidine-6-carbonitrile (6).** A mixture of compound 1 (0.256 g, 1 mmol) and ethyl chloroacetate (0.1 g, 1.2 mmol) in ethanol (5 ml) and a few drops of triethylamine was allowed to reflux for 6 h; after that, the reaction mixture was cooled. The precipitated solid product was filtered off, washed with ethanol, dried, and recrystallized from ethanol to afford a pale yellow powder (yield: 55%) m.p. over 265–270°C. IR (KBr,  $\nu$ ,  $\text{cm}^{-1}$ ): 3131–2966 (CH for aromatic and aliphatic), 2229 (CN), 1675, 1615 (2 C=O). <sup>1</sup>H-NMR (DMSO- $d_6$ , 500 MHz):  $\delta$  = 2.49 (d, 1H, CH(CN)-CH(Ar)) 3.36 (s, 1H, J =, methine-CH(CN)), 3.99 (s, 2H, CH<sub>2</sub>thiazole ring) 7.739, 7.951 (d, d, 4H, CH Aromatic) ppm. Anal. Calcd. for  $\text{C}_{14}\text{H}_8\text{N}_4\text{O}_2\text{S}$  (296.30): C, 56.75; H, 2.72; N, 18.91; S, 10.82.

**(E)-2-benzylidene-7-(4-cyanophenyl)-3,5-dioxo-2,3,6,7-tetrahydro-5H-thiazolo[3,2-a]pyrimidine-6-carbonitrile (7).** A mixture of Compound 1 (0.256 g, 1 mmol), chloroacetic acid (0.113 g, 1.2 mmol), benzaldehyde (0.127 g, 1.2 mmol), and anhydrous sodium acetate (0.328 g, 4 mmol) in a mixture of acetic acid and acetic anhydride (1:1) was heated under reflux for 7 h. The formed solid was collected and washed with acetic acid and ethanol several times, dried, and recrystallized from ethanol to give a greenish-yellow powder (yield: 60%) m.p. 270–275°C. IR (KBr,  $\nu$ ,  $\text{cm}^{-1}$ ): 2228 (CN), 1761, 1694 (2 C=O). <sup>1</sup>H-NMR (DMSO- $d_6$ , 500 MHz):  $\delta$  = 2.49 (d, 1H, CH(CN)-CH(Ar)) 3.35 (s, 1H, J =, methine-CH(CN)), 4.5 (s, 1H, C=CH benzylidene), 7.771, 7.787 (m, 9H, aromatic) ppm. Anal. Calcd. for  $\text{C}_{21}\text{H}_{12}\text{N}_4\text{O}_2\text{S}$  (384.41): C, 65.61; H, 3.15; N, 14.57; S, 8.34.

**2-(Benzo[d]thiazol-2-ylamino)-4-(4-cyanophenyl)-6-oxo-1,4,5,6-tetrahydro pyrimidine-5-carbonitrile (8).** A mixture of Compound (2) (0.27 g, 1 mmol) and 2-aminobenzothiazole (0.15 g, 1 mmol) in ethanol (10 ml) and a few drops of triethylamine was refluxed for 5 h, then cooled at room temperature. After that, the reaction mixture was poured into ice water. The precipitated solid product was filtered off, washed with ethanol, dried, and recrystallized from ethanol to afford a pale brown powder (yield: 70%) m.p. 285–290°C. IR (KBr,  $\nu$ ,  $\text{cm}^{-1}$ ): 3448, 3422 (2 NH, str), 3099–2926 (CH for aromatic and aliphatic), 2230 (CN), 1676 (C=O). <sup>1</sup>H-NMR (DMSO- $d_6$ , 500 MHz):  $\delta$  = 3.06 (d, 1H, J =, CH(CN)-CH(Ar)), 3.48 (s, 1H, J =, methine-CH(CN)), 9.92, 11.95 (s, 2H, 2 NH, str) 7.85–7.47 (m, 8H, CH Aromatic) ppm. Anal. Calcd. for  $\text{C}_{19}\text{H}_{12}\text{N}_6\text{OS}$  (372.08): C, 61.28; H, 3.25; N, 22.57; S, 8.61.

**4-(4-Cyanophenyl)-6-oxo-2-(2-phenylhydrazine)-1,4,5,6-tetrahydro pyrimidine-5-carbonitrile (9).** A mixture of Compound (2) (0.27 g, 1 mmol) and phenyl-hydrazine (0.108 g, 1 mmol) in ethanol (10 ml) and a few drops of triethylamine was refluxed for 4 h, then cooled at room temperature. After that, the reaction mixture was poured into ice water. The precipitated solid product was filtered off, washed with ethanol, dried, and recrystallized from ethanol to afford a pale brown powder (yield: 55%) m.p. over 300°C. IR (KBr,  $\nu$ ,  $\text{cm}^{-1}$ ): 3449 (NH, str), 2224 (CN), 1669 (C=O). <sup>1</sup>H-NMR (DMSO- $d_6$ , 500 MHz):  $\delta$  = 2.62 (d, 1H, J =, CH(CN)-CH(Ar)), 3.37 (s, 1H, J =, methine-CH(CN)), 8.205–8.189 (d, d, 2H, 2 NH, str) 8.002 (s, 1H, NH, str) 7.693–7.624 (m, 9H, CH aromatic) ppm. Anal. Calcd. for  $\text{C}_{18}\text{H}_{14}\text{N}_6\text{O}$  (330.35): C, 65.44; H, 4.27; N, 25.44.



### 3.7. Biology

#### 3.7.1 Evaluation of antioxidant activity by DPPH radical scavenging

**method.** Different compounds' free radical scavenging activity was measured by 1, 1-diphenyl-2-picryl hydroxyl (DPPH). In brief, a 0.1 mM solution of DPPH in ethanol was prepared. This solution (1 ml) was added to 3 ml. of the different compounds in ethanol at various concentrations (3.9, 7.8, 15.62, 31.25, 62.5, 125, 250, 500, 1000 µg/ml). Here, only those compounds solubilized in ethanol and their various concentrations were prepared by dilution [38]. The mixture was shaken vigorously and allowed to stand at room temperature for 30 minutes. Then, absorbance was measured at 517 nm by using a spectrophotometer (UV-VIS Milton Roy). The reference standard compound used was ascorbic acid, and the experiment was done in triplicate. The IC<sub>50</sub> value of the sample, which is the concentration of sample required to inhibit 50% of the DPPH free radical, was calculated using the Log dose inhibition curve. The lower absorbance of the reaction mixture indicates higher free radical activity. The percent DPPH scavenging effect was calculated using the following equation: DPPH scavenging effect (%), or percent inhibition =  $A_0 - A_1 / A_0 \times 100$ . A<sub>0</sub> is the absorbance of the control reaction, and A<sub>1</sub> is the absorbance in the presence of a test or standard sample [39].

**3.7.2 Hemolytic assay.** The hemolytic assay was performed using the method reported in [37,40,41]. Freshly collected human red blood cells were washed thrice with 150 mM NaCl (2500 rpm for 10 minutes). The plasma was removed, and the cells were suspended in phosphate buffer saline (pH 7.4) for 2% RBC concentration. Double-folded dilution concentrations (1000, 800, 600, 400, 200, 100, 50 µg/ml) of the compound were mixed with 2% L of RBC solutions, and the final reaction mixture volume was measured up to 1 ml by adding PBS. The reaction mixture was then placed in the water bath for 1 hour at 37°C. After incubation, the reaction mixture was centrifuged at 2500 rpm for 15 minutes. The supernatant was collected, and the optical density was measured at 541 nm, keeping the phosphate buffer saline blank. Deionized water was used as a positive control. The experiment was carried out in triplicate, and the mean ± SD was calculated.

$$\text{Percentage of hemolysis} = \frac{(\text{Absorbance of sample} - \text{Absorbance of blank}) \times 100}{\text{Absorbance of positive control}}$$

### 3.8 In-silico studies

**3.8.1 Molecular docking.** The docking analyses were carried out and characterized by the Molecular Environment (MOE), ChemDraw 16 compound preparation, Chem3D structures, and Chem 3D 16 (Molecular Modeling and Analysis; Cambridge Soft Corporation) software. To dock the co-crystal structure of the COX-2 complex with SC-558, a selective COX-2 blocker was acquired from the PDB (protein data bank) **PDB: 1CX2** and co-crystallized with ascorbic acid as a reference ligand isolated from cytochrome c peroxidase enzyme **PDB: 2X08**. After the crystal structure was downloaded from the PDB [www.rcsb.org](http://www.rcsb.org), the water molecules, co-ligand, and metal ions were removed [42–44].

The final form was obtained after 3D protonation and the correction process. The MOE site finder generated the active binding sites to create the dummy sites as the binding pocket. The default docking parameters were triangle matches for replacing the molecule and London dG for rescoring the docking scores. The DFT-optimized structures of the compounds were used to generate the five best binding poses with flexible molecule rotation. The hydrogen bonds formed between the elastase and the investigated compound were used to rank the binding affinity and

were presented as the free binding energy (*S*, kcal/mol). The higher negative values of the docking scores were presented along with 2D and 3D structures [45,46].

### 3.8.2 Pharmacokinetics.

**LabMol and ProTox-II.** Computational toxicity estimations are faster than determining toxic doses in animals and also help reduce the number of animal experiments. Toxic doses are often given as LD<sub>50</sub> in mg/kg body weight. The LD<sub>50</sub> is the median lethal dose at which 50% of test subjects die upon exposure to a compound. Toxicity classes are defined according to the globally harmonized system of classification and labeling of chemicals (GHS) [47].

LD<sub>50</sub> values are given in [mg/kg]:

- 1- Class I: fatal if swallowed ( $LD_{50} \leq 5$ ).
- 2- Class II: fatal if swallowed ( $5 < LD_{50} \leq 50$ ).
- 3- Class III: toxic if swallowed ( $50 < LD_{50} \leq 300$ ).
- 4- Class IV: harmful if swallowed ( $300 < LD_{50} \leq 2000$ ).
- 5- Class V: may be harmful if swallowed ( $2000 < LD_{50} \leq 5000$ )
- 6- Class VI: non-toxic ( $LD_{50} > 5000$ )

The ProTox-II software predicts different toxicity endpoints, such as acute toxicity, hepatotoxicity, carcinogenicity, and mutagenicity [48]. The Pred-hERG (human Ether-a-go-go-Related Gene) software was used to assess cardiotoxicity. The software depends on statistically significant and externally predictive quantitative structure-activity relationship (QSAR) models of hERG blockage closely associated with severe and potentially fatal cardiac dysrhythmia. The SDF (structure data file) and SMILES (simplified molecular-input line-entry system) strings were used throughout the generation process [48].

### Molinspiration.

**Bioavailability radar** This is a tool for rapid appraisal of the drug-likeness of a molecule. Six physicochemical properties (lipophilicity, size, polarity, solubility, flexibility, and saturation) were considered. On each axis, a physicochemical range was determined by descriptors as previously explained [49] and illustrated as a pink area in which the radar plot of the compound must fall in its entirety to be considered drug-like. Pro-Tox-II carried this out.

**Physicochemical properties** Physicochemical properties include simple molecular and physicochemical descriptors such as molecular weight (MW), number of specific atom types, fraction Csp<sup>3</sup> (carbon bond saturation as defined by fraction sp<sup>3</sup>), which measure the complexity of the molecule, number of particular bond types, and molecular refractivity (MR). Also, the topological polar surface area (TPSA) was used to calculate the polar surface area (PSA), which quickly estimates some ADME properties, especially concerning the ability to pass through biological barriers like the blood-brain barrier [50].

**Lipophilicity** Lipophilicity was described by calculating the partition coefficient between *n*-octanol and water (Log *P*<sub>o/w</sub>). Then, Molinspiration gave access to five free predictors, iLOGP, XLOGP3, WLOGP, MLOGP, and SILICO—IT, to generate the consensus log *P*<sub>o/w</sub>, which is the mean of the predicted values [51].

**Water solubility** Molinspiration predicts water solubility [52]. The output is the Log *S* values, the decimal Log *p* of the molar solubility in water. In addition, the water solubility was provided in mg/ml and mol/l, as were the qualitative solubility classes.

**Pharmacokinetics** Molinspiration uses specialized models to evaluate the ADME behaviors of the test compound. Lipinski's rule of five (5) by Christopher A. Lipinski 1997 is a rule of thumb for assessing drug-likeness and determining if an inhibitor with specific biological and pharmacological properties would be an orally active drug in the human body. The rule states

that a molecule can be orally absorbed/active if two (2) or more of these thresholds obtain: molecular weight (Mw) of molecule < 500, octanol/water partition coefficient (log P) ≤ 5, number of hydrogen bond acceptors (nHBA) ≤ 10, number of hydrogen bond donors (nHBD) ≤ 5, and topological polar surface area (TPSA) < 40 Å<sup>2</sup>, must not be violated. The first model predicts passive gastrointestinal absorption and penetration of the blood-brain barrier (BBB) [53]. The second model predicts being substrate or non-substrate of the permeability glycoprotein (P-GP), essential to evaluate active efflux through membranes, e.g., from the gastrointestinal wall to the lumen or brain [41]. The third model predicts the interaction of compounds with the cytochrome P450 (CYP) major isoenzymes (CYP1A2, CYP2C19, CYP2C9, CYP2D6, CYP3A4), which is an essential contributor to drug elimination through metabolic biotransformation. Also, inhibition of these isoenzymes is a cause of drug interactions [37], leading to toxic or other adverse effects. The fourth model predicts the skin permeability coefficient (K<sub>p</sub>), which linearly correlates with molecular size and lipophilicity [54]—the more negative the log K<sub>p</sub>(cm/s), the less skin permeation.

**3.8.3 DFT.** The Spartan '14 program was used to perform quantum chemistry calculations using the DFT method. In addition, spartan '20 was used to display all the data files. The density functional theory (DFT) at 6-311G<sup>++</sup>(d,p) basis set/B3LYP approach was utilized to optimize the organic chemical structure of the compounds under investigation, and Chem3D 16.0 software was used to create the original chemical structure [53,54].

## Conclusion

A cost-effective and eco-friendly protocol has been developed by using the Biginelli synthesis of 4-cyanobenzaldehyde, ethyl cyanoacetate, and thiourea in the presence of TiO<sub>2</sub> nanoparticles to yield 4-(4-cyanophenyl)-6-oxo-2-thioxohexahydropyrimidine-5-carbonitrile (1). This multi-component system is safe and non-toxic. Compound (1) was reacted with different reagents, as listed above, to produce new compounds. These compounds were then studied for inflammatory and antioxidant activity. Compounds (5) and (8) showed great activity with IC<sub>50</sub>. The in-silico studies include molecular docking using MOE and pharmacokinetics using Toxopredict, SAR, and DFT studies.

## Supporting information

**S1 Fig.** 4-(4-cyanophenyl)-6-oxo-2-thioxohexahydropyrimidine-5-carbonitrile (1):  
(PDF)

**S2 Fig.** 4-(4-Cyanophenyl)-2-(methylthio)-6-oxo-1,4,5,6-tetrahydropyrimidine-5-carbonitrile (2):  
(PDF)

**S3 Fig.** 2-((cyanomethyl)thio)-4-(4-cyanophenyl)-6-oxo-1,4,5,6-tetrahydropyrimidine-5-carbonitrile (3)  
(PDF)

**S4 Fig.** 4-(4-cyanophenyl)-6-oxo-2-((2-oxopropyl)thio)-1,4,5,6-tetrahydropyrimidine-5-carbonitrile (4):  
(PDF)

**S5 Fig.** 4-Amino-8-(4-cyanophenyl)-6-oxo-7,8-dihydro-2H,6H-pyrimido[2,1-b][1,3]thiazine-7-carbonitrile (5)  
(PDF)

**S6 Fig. 7-(4-Cyanophenyl)-3,5-dioxo-2,3,6,7-tetrahydro-5H-thiazolo[3,2-a]pyrimidine-6-carbonitrile (6)**

(PDF)

**S7 Fig. (E)-2-benzylidene-7-(4-cyanophenyl)-3,5-dioxo-2,3,6,7-tetrahydro-5H-thiazolo[3,2-a]pyrimidine-6-carbonitrile (7)**

(PDF)

**S8 Fig. 2-(Benzo[d]thiazol-2-ylamino)-4-(4-cyanophenyl)-6-oxo-1,4,5,6-tetrahydropyrimidine-5-carbonitrile (8)**

(PDF)

**S9 Fig. 4-(4-Cyanophenyl)-6-oxo-2-(2-phenylhydrazineyl)-1,4,5,6-tetrahydropyrimidine-5-carbonitrile (9)**

(PDF)

**S1 Graphical Abstract. New pyrimidine candidates, antioxidant activity, anti-inflammatory effects, and insilico-studies.**

(PPTX)

## Acknowledgments

The authors introduce their thanks to Taif University Saudi Arabia for supporting this work through project number TU-DSPP-2024-19.

## Author contributions

**Conceptualization:** Wesam S. Shehab, Hend A. Haikal.

**Data curation:** Abdel Rahman B.A. El-Gazzar, Hend A. Haikal, Samar M. Mouneir.

**Formal analysis:** Abdel Rahman B.A. El-Gazzar, Hend A. Haikal, Samar M. Mouneir, Abdul-Hamid M. Emwas.

**Funding acquisition:** Abdul-Hamid M. Emwas, Mariusz Jaremko.

**Investigation:** Hend A. Haikal, Mariusz Jaremko.

**Methodology:** Samar M. Mouneir.

**Project administration:** Wesam S. Shehab, Magda H. Abdellattif.

**Resources:** Ahmed F. EL-Faragy, Abdel Rahman B.A. El-Gazzar, Abdul-Hamid M. Emwas.

**Software:** Ahmed F. EL-Faragy, Magda H. Abdellattif.

**Supervision:** Wesam S. Shehab, Ahmed F. EL-Faragy.

**Validation:** Abdel Rahman B.A. El-Gazzar, Mariusz Jaremko, Magda H. Abdellattif.

**Writing – original draft:** Wesam S. Shehab.

**Writing – review & editing:** Abdul-Hamid M. Emwas, Magda H. Abdellattif.

## References

1. Leng Y, Liu J, Jiang P, Wang J. Organometallic-polyoxometalate hybrid based on V-Schiff base and phosphovanadomolybdate as a highly effective heterogenous catalyst for hydroxylation of benzene. *Chem. Eng. J.* 2014;239:1–7. <https://doi.org/10.1016/j.cej.2013.10.092>
2. AbdEl-Azim MHM, Aziz MA, Mouneir SM, El-Faragy AF, Shehab WS. Ecofriendly synthesis of pyrano[2,3-d]pyrimidine derivatives and related heterocycles with anti-inflammatory activities. *Arch Pharm (Weinheim)*. 2020;353(9):e2000084. <https://doi.org/10.1002/ardp.202000084> PMID: [32583459](https://pubmed.ncbi.nlm.nih.gov/32583459/)

3. Shehab WS, EL-Faragy AF, Abdelhamid AO, Aziz MA. Synthesis and biological application of pyranopyrimidine derivatives catalyzed by efficient nanoparticles and their nucleoside analogues. *Synth. Commun.* 2019;49(24):3560–72. <https://doi.org/10.1080/00397911.2019.1679538>
4. Shehab WS, Abdellattif MH, Mouneir SM. Heterocyclization of polarized system: synthesis, antioxidant and anti-inflammatory 4-(pyridin-3-yl)-6-(thiophen-2-yl) pyrimidine-2-thiol derivatives. *Chem Cent J.* 2018;12(1):68. <https://doi.org/10.1186/s13065-018-0437-y> PMID: 29881977
5. Aziz MA, Shehab WS, Al-Karmalawy AA, El-Faragy AF, Abdellattif MH. Design, synthesis, biological evaluation, 2D-QSAR modeling, and molecular docking studies of novel 1H-3-indolyl derivatives as significant antioxidants. *Int J Mol Sci.* 2021;22(19):10396. <https://doi.org/10.3390/ijms221910396> PMID: 34638734
6. Tylińska B, Wiatrak B, Czyżnikowska Ż, Cieśla-Niechwiadowicz A, Gębarowska E, Janicka-Kłos A. Novel pyrimidine derivatives as potential anticancer agents: synthesis, biological evaluation and molecular docking study. *Int J Mol Sci.* 2021;22(8):3825. <https://doi.org/10.3390/ijms22083825> PMID: 33917090
7. Salem MM, Gerges MN, Noser AA. Synthesis, molecular docking, and in-vitro studies of pyrimidine-2-thione derivatives as antineoplastic agents via potential RAS/PI3K/Akt/JNK inhibition in breast carcinoma cells. *Sci Rep.* 2022;12(1):22146. <https://doi.org/10.1038/s41598-022-26571-7> PMID: 36550279
8. Metwally NH, Radwan IT, El-Serwy WS, Mohamed MA. Design, synthesis, DNA assessment and molecular docking study of novel 2-(pyridin-2-ylimino)thiazolidin-4-one derivatives as potent antifungal agents. *Bioorg Chem.* 2019;84:456–67. <https://doi.org/10.1016/j.bioorg.2018.11.050> PMID: 30576909
9. Marinescu M. Biginelli reaction mediated synthesis of antimicrobial pyrimidine derivatives and their therapeutic properties. *Molecules.* 2021;26(19):6022. <https://doi.org/10.3390/molecules26196022> PMID: 34641566
10. Ali T, Wang H, Iqbal W, Bashir T, Shah R, Hu Y. Electro-synthesis of organic compounds with heterogeneous catalysis. *Adv Sci (Weinh).* 2022;10(1):e2205077. <https://doi.org/10.1002/advs.202205077> PMID: 36398622
11. da Silva MJ, Rodrigues AA, Lopes NPG. Cesium heteropolyacid salts: synthesis, characterization and activity of the solid and versatile heterogeneous catalysts. *Chemistry.* 2023;5(1):662–90. <https://doi.org/10.3390/chemistry5010047>
12. Statkiewicz M, Maryan N, Kulecka M, Kuklinska U, Ostrowski J, Mikula M. Functional analyses of a low-penetrance risk variant rs6702619/1p21.2 associating with colorectal cancer in Polish population. *Acta Biochim Pol.* 2019;66(3):329–36. [https://doi.org/10.18388/abp.2019\\_2775](https://doi.org/10.18388/abp.2019_2775) PMID: 31531420
13. Patel A, Shah J, Patel K, Patel K, Patel H, Dobaria D, et al. Ultrasound-assisted one-pot synthesis of tetrahydropyrimidine derivatives through biginelli condensation: a catalyst free green chemistry approach. *LOC.* 2021;18(9):749–56. <https://doi.org/10.2174/1570178617999201105162851>
14. Patel A, Gandhi K, Shah S, Patel D, Chhatbar S, Shah D, et al. *In silico* study and solvent-free one-pot synthesis of tetrahydropyrimidine derivatives by mechanochemistry approach for targeting human neutrophil elastase against lung cancer. *Curr Comput Aided Drug Des.* 2022;18(4):293–306. <https://doi.org/10.2174/1573409918666220622232501> PMID: 35747983
15. Li X, Fu L, Chen F, Zhao S, Zhu J, Yin C. Application of heterogeneous catalytic ozonation in wastewater treatment: an overview. *Catalysts.* 2023;13(2):342. <https://doi.org/10.3390/catal13020342>
16. Patil TP, Vibhute AA, Patil SL, Dongale TD, Tiwari AP. Green synthesis of gold nanoparticles via Capsicum annum fruit extract: Characterization, antiangiogenic, antioxidant and anti-inflammatory activities. *Appl Surf Sci Adv.* 2023;13:100372. <https://doi.org/10.1016/j.apsadv.2023.100372>
17. Liu N, Zhang P, Xue M, Zhang M, Xiao Z, Xu C, et al. Anti-inflammatory and antioxidant properties of rice bran oil extract in copper sulfate-induced inflammation in zebrafish (*Danio rerio*). *Fish Shellfish Immunol.* 2023;136:108740. <https://doi.org/10.1016/j.fsi.2023.108740> PMID: 37061070
18. Bayrak H, Fahim AM, Yaylaci Karahalil F, Azafad I, Boyraci GM, Taflan E. Synthesis, antioxidant activity, docking simulation, and computational investigation of novel heterocyclic compounds and Schiff bases from picric acid. *J. Mol. Struct.* 2023;1281:135184. <https://doi.org/10.1016/j.molstruc.2023.135184>
19. Meng C-W, Zhao H-Y, Zhu H, Peng C, Zhou Q-M, Xiong L. Novel indane derivatives with antioxidant activity from the roots of *Anisodus tanguticus*. *Molecules.* 2023;28(3):1493. <https://doi.org/10.3390/molecules28031493> PMID: 36771160
20. Saleem TKM, Azeem AK, Dilip C, Sankar C, Prasanth NV, Duraisami R. Anti-inflammatory activity of the leaf extracts of *Gendarussa vulgaris* Nees. *Asian Pac J Trop Biomed.* 2011;1(2):147–9. [https://doi.org/10.1016/S2221-1691\(11\)60014-2](https://doi.org/10.1016/S2221-1691(11)60014-2) PMID: 23569746



21. Pfefferlé M, Ingoglia G, Schaer CA, Yalamanoglu A, Buzzi R, Dubach IL, et al. Hemolysis transforms liver macrophages into antiinflammatory erythrophagocytes. *J Clin Invest*. 2020;130(10):5576–90. <https://doi.org/10.1172/JCI137282> PMID: 32663195
22. Abdelghany TM, Al-Rajhi AMH, Almuhayawi MS, Abada E, Al Abboud MA, Moawad H, et al. Green fabrication of nanocomposite doped with selenium nanoparticle-based starch and glycogen with its therapeutic activity: antimicrobial, antioxidant, and anti-inflammatory in vitro. *Biomass Conv Bioref*. 2022;13(1):431–43. <https://doi.org/10.1007/s13399-022-03257-8>
23. Elbestawy MKM, El-Sherbiny GM, Moghannem SA. Antibacterial, antibiofilm and anti-inflammatory activities of eugenol clove essential oil against resistant *Helicobacter pylori*. *Molecules*. 2023;28(6):2448. <https://doi.org/10.3390/molecules28062448> PMID: 36985419
24. Bharathi R, Santhi N. Molecular docking analysis of selected pyrimidine derivatives with human cyclin-dependent kinase 2. *Bioinformation*. 2021;17(7):680–5. <https://doi.org/10.6026/97320630017680> PMID: 35283581
25. Abdellatif MH, Elkamhawy A, Hagar M, Hadda TB, Shehab WS, Mansy W, et al. Novel saccharin analogs as promising antibacterial and anticancer agents: synthesis, DFT, POM analysis, molecular docking, molecular dynamic simulations, and cell-based assay. *Front Pharmacol*. 2022;13:958379. <https://doi.org/10.3389/fphar.2022.958379> PMID: 36267293
26. Belal A, Elanany MA, Al-Karmalawy AA, Elkamhawy A, Abourehab MAS, Ghamry HI, et al. Design of new captopril mimics as promising ACE inhibitors: ADME, pharmacophore, molecular docking and dynamics simulation with MM-PBSA and PCA calculations. *J Taibah Univ Sci*. 2023;17(1). <https://doi.org/10.1080/16583655.2023.2210348>
27. Li B, Wang X, Yan M, Li L. Preparation and characterization of nano-TiO<sub>2</sub> powder. *Mater. Chem. Phys*. 2003;78(1):184–8. [https://doi.org/10.1016/s0254-0584\(02\)00226-2](https://doi.org/10.1016/s0254-0584(02)00226-2)
28. Hung W-C, Chen Y-C, Chu H, Tseng T-K. Synthesis and characterization of TiO<sub>2</sub> and Fe/TiO<sub>2</sub> nanoparticles and their performance for photocatalytic degradation of 1,2-dichloroethane. *Appl. Surf. Sci*. 2008;255(5):2205–13. <https://doi.org/10.1016/j.apsusc.2008.07.079>
29. El-Morsy MA, Awwad NS, Ibrahim HA, Farea MO. Optical, and electrical conductivity properties of ZnO and TiO<sub>2</sub> nanoparticles scattered in PEO-PVA for electrical devices. *Results Phys*. 2023;50:106592. <https://doi.org/10.1016/j.rinp.2023.106592>
30. El-Aziz MEA, Youssef AM, Kamal KH, Kelnar I, Kamel S. Preparation and performance of bionano-composites based on grafted chitosan, GO and TiO<sub>2</sub>-NPs for removal of lead ions and basic-red 46. *Carbohydr Polym*. 2023;305:120571. <https://doi.org/10.1016/j.carbpol.2023.120571> PMID: 36737211
31. Nam T-G, Nara SJ, Zagol-Ikapitte I, Cooper T, Valgimigli L, Oates JA, et al. Pyridine and pyrimidine analogs of acetaminophen as inhibitors of lipid peroxidation and cyclooxygenase and lipoxigenase catalysis. *Org Biomol Chem*. 2009;7(24):5103–12. <https://doi.org/10.1039/b912528k> PMID: 20024105
32. Sayed AI, Mansour YE, Ali MA, Aly O, Khoder ZM, Said AM, et al. Novel pyrrolopyrimidine derivatives: design, synthesis, molecular docking, molecular simulations and biological evaluations as antioxidant and anti-inflammatory agents. *J Enzyme Inhib Med Chem*. 2022;37(1):1821–37. <https://doi.org/10.1080/14756366.2022.2090546> PMID: 35762086
33. Dudhe R, Sharma PK, Verma PK. Pyrimidine containing furanose derivative having antifungal, antioxidant, and anticancer activity. *Org Med Chem Lett*. 2014;4(1):3. <https://doi.org/10.1186/s13588-014-0003-0> PMID: 26054922
34. Alijagic A, Gaglio D, Napodano E, Russo R, Costa C, Benada O, et al. Titanium dioxide nanoparticles temporarily influence the sea urchin immunological state suppressing inflammatory-related gene transcription and boosting antioxidant metabolic activity. *J Hazard Mater*. 2020;384:121389. <https://doi.org/10.1016/j.jhazmat.2019.121389> PMID: 31639584
35. Rashid HU, Martines MAU, Duarte AP, Jorge J, Rasool S, Muhammad R, et al. Research developments in the syntheses, anti-inflammatory activities and structure-activity relationships of pyrimidines. *RSC Adv*. 2021;11(11):6060–98. <https://doi.org/10.1039/d0ra10657g> PMID: 35423143
36. Tageldin GN, Fahmy SM, Ashour HM, Khalil MA, Nassra RA, Labouta IM. Design, synthesis and evaluation of some pyrazolo[3,4-d]pyrimidine derivatives bearing thiazolidinone moiety as anti-inflammatory agents. *Bioorg Chem*. 2018;80:164–73. <https://doi.org/10.1016/j.bioorg.2018.06.013> PMID: 29929077
37. Ammar YA, Micky JA, Aboul-Magd DS, Abd El-Hafez SMA, Hessein SA, Ali AM, et al. Development and radiosterilization of new hydrazono-quinoline hybrids as DNA gyrase and topoisomerase IV inhibitors: Antimicrobial and hemolytic activities against uropathogenic isolates with molecular docking study. *Chem Biol Drug Des*. 2023;101(2):245–70. <https://doi.org/10.1111/cbdd.14154> PMID: 36305722

38. Bluhm U, Boucher J-L, Buss U, Clement B, Friedrich F, Girreser U, et al. Synthesis and evaluation of pyrido[1,2-a]pyrimidines as inhibitors of nitric oxide synthases. *Eur J Med Chem*. 2009;44(7):2877–87. <https://doi.org/10.1016/j.ejmech.2008.12.007> PMID: 19144449
39. Bulmus V, Woodward M, Lin L, Murthy N, Stayton P, Hoffman A. A new pH-responsive and glutathione-reactive, endosomal membrane-disruptive polymeric carrier for intracellular delivery of biomolecular drugs. *J Control Release*. 2003;93(2):105–20. <https://doi.org/10.1016/j.jconrel.2003.06.001> PMID: 14636717
40. Bouamrane OL, Hellal A, Hachama K, Touafri L, Haddadi I, Layaida H, et al. Effect of the bifunctionalization of aminomethylphosphonic acid on the structural, electronic, vibrational, thermodynamic and antioxidant activity: microwave-assisted synthesis, Density Functional Theory studies and DPPH radical scavenging activity. *J. Mol. Struct.* 2022;1250:131714. <https://doi.org/10.1016/j.molstruc.2021.131714>
41. Sæbø IP, Bjørås M, Franzyk H, Helgesen E, Booth JA. Optimization of the hemolysis assay for the assessment of cytotoxicity. *Int J Mol Sci*. 2023;24(3):2914. <https://doi.org/10.3390/ijms24032914> PMID: 36769243
42. Kothayer H, Rezq S, Abdelkhalek AS, Romero DG, Elbaramawi SS. Triple targeting of mutant EGFR L858R/T790M, COX-2, and 15-LOX: design and synthesis of novel quinazolinone tethered phenyl urea derivatives for anti-inflammatory and anticancer evaluation. *J Enzyme Inhib Med Chem*. 2023;38(1):2199166. <https://doi.org/10.1080/14756366.2023.2199166> PMID: 37038884
43. Shehab WS, Abdelaziz M, Elhoseni NKR, Assy MG, Abdellatif MH, Hamed EO. Design, synthesis, molecular docking, and evaluation antioxidant and antimicrobial activities for novel 3-Phenylimidazolidin-4-One and 2-aminothiazol-4-one derivatives. *Molecules*. 2022;27(3):767. <https://doi.org/10.3390/molecules27030767> PMID: 35164032
44. Gomha SM, Riyadh SM, Huwaimel B, Zayed MEM, Abdellatif MH. Synthesis, molecular docking study, and cytotoxic activity against MCF cells of new thiazole-thiophene scaffolds. *Molecules*. 2022;27(14):4639. <https://doi.org/10.3390/molecules27144639> PMID: 35889511
45. Abdellatif MH, Abdel-Rahman AAH, Arief MMH, Mounieir SM, Ali A, Hussien MA, Okasha RM, Afifi TH, Hagar M. Novel 2-Hydroselenonicotinonitriles and Selenopheno[2, 3-b]pyridines: Efficient Synthesis, Molecular Docking-DFT Modeling, and Antimicrobial Assessment. *ProTox-II - Prediction of TOXicity of chemicals*.
46. Murad HAS, Alqurashi TMA, Hussien MA. Interactions of selected cardiovascular active natural compounds with CXCR4 and CXCR7 receptors: a molecular docking, molecular dynamics, and pharmacokinetic/toxicity prediction study. *BMC Complement Med Ther*. 2022;22(1):35. <https://doi.org/10.1186/s12906-021-03488-8> PMID: 35120520
47. Mottin M, Caesar LK, Brodsky D, Mesquita NCMR, de Oliveira KZ, Noske GD, et al. Chalcones from *Angelica keiskei* (ashitaba) inhibit key Zika virus replication proteins. *Bioorg Chem*. 2022;120:105649. <https://doi.org/10.1016/j.bioorg.2022.105649> PMID: 35124513
48. Verheij HJ. Leadlikeness and structural diversity of synthetic screening libraries. *Mol Divers*. 2006;10(3):377–88. <https://doi.org/10.1007/s11030-006-9040-6> PMID: 17031539
49. Ghose AK, Viswanadhan VN, Wendoloski JJ. A knowledge-based approach in designing combinatorial or medicinal chemistry libraries for drug discovery. 1. A qualitative and quantitative characterization of known drug databases. *J Comb Chem*. 1999;1(1):55–68. <https://doi.org/10.1021/cc9800071> PMID: 10746014
50. Veber DF, Johnson SR, Cheng H-Y, Smith BR, Ward KW, Kopple KD. Molecular properties that influence the oral bioavailability of drug candidates. *J Med Chem*. 2002;45(12):2615–23. <https://doi.org/10.1021/jm020017n> PMID: 12036371
51. Martin YC. A bioavailability score. *J Med Chem*. 2005;48(9):3164–70. <https://doi.org/10.1021/jm0492002> PMID: 15857122
52. Lipinski CA, Lombardo F, Dominy BW, Feeney PJ. Experimental and computational approaches to estimate solubility and permeability in drug discovery and development settings. *Adv. Drug Deliv. Rev*. 1997;23(1–3):3–25. [https://doi.org/10.1016/s0169-409x\(96\)00423-1](https://doi.org/10.1016/s0169-409x(96)00423-1)
53. Ertl P, Schuffenhauer A. Estimation of synthetic accessibility score of drug-like molecules based on molecular complexity and fragment contributions. *J Cheminform*. 2009;1(1):8. <https://doi.org/10.1186/1758-2946-1-8> PMID: 20298526
54. Legler CR, Brown NR, Dunbar RA, Harness MD, Nguyen K, Oyewole O, et al. Scaled quantum mechanical scale factors for vibrational calculations using alternate polarized and augmented basis sets with the B3LYP density functional calculation model. *Spectrochim Acta A Mol Biomol Spectrosc*. 2015;145:5–24. <https://doi.org/10.1016/j.saa.2015.02.103>